ABSTRACT

Title of Thesis: PRODUCTION OF HIGH SURFACE AREA SILICA PARTICLES BY ACOUSTODISPERSION PRECIPITATION

Degree Candidate: Jermey Norman Augustus Matthews

Degree and year: Master of Science, 2004

Thesis directed by: Professor Michael T. Harris
Department of Chemical Engineering

A continuous Acoustodispersion Precipitation Reaction (APR) flow process was applied to the production of high surface area silica particles. An ultrasonic reactor was used to atomize and disperse silica gel into a drying chamber for further solidification. Upon particle synthesis, the resulting powder was analyzed The effect of sodium silicate concentration, volumetric flow rate through the ultrasonic nozzle, and drying temperature on particle diameter and specific surface area (A_{sp}) was observed. A mathematical equation was derived using the Box-Behnken statistical design.

SEM imaging was employed in measuring the particle size and observing the morphology, and BET theory was exploited in collecting surface area data. SEM images showed porous and spherical silica particles. The number average diameter of the particles ranged from 13.155

μm. Most of the A_{sp} values ranged from 100 – 300 m^2/g. The highest A_{sp} achieved was 342 m^2/g and the lowest was 19.9 m^2/g.

PRODUCTION OF HIGH SURFACE AREA SILICA PARTICLES BY ACOUSTODISPERSION PRECIPITATION

by

Jermey Norman Augustus Matthews

Thesis submitted to the Faculty of the Graduate School of the
University of Maryland, College Park in partial fulfillment
of the requirements for the degree of
Master of Science
2004

Advisory Committee:

Professor Michael T. Harris, Chair
Professor Sheryl H. Ehrman
Professor Sandra C. Greer

DEDICATION

I would like to dedicate this work to my dear parents, Dr. Lionel and Mrs. Walterine Matthews. Their lessons and example on diligence, discipline, and determination, are major contributors to any success that I may achieve in life – including this scholarly work.

ACKNOWLEDGEMENTS

First and foremost to my Lord and Savior Jesus Christ, thank you for giving me wisdom and strength.

Dr. Michael Harris, my advisor, comes first in my acknowledgements, as he was the catalyst that drove me when I faced seemingly insurmountable energy barriers of ignorance and doubt. The patience and willingness of my committee members, Professor Ehrman and Professor Greer is also recognized and duly appreciated.

Other figures that deserve mention are Dr. Otto Wilson and Dr. Isabel Lloyd, who gave me permission to use the NOVA 1200 particle analyzer, and Quyhn Nguyen who trained me to use it. I thank Mr. Tim Maugel who helped me tremendously with the SEM analysis, and Mr. Edd Cole, who was instrumental in the design of the mixing and drying chambers. I am grateful to my undergraduate research assistants, Patrick Taylor and Natasha Prokharenko, for helping me to get over the experimental hump in crunch time. My gratitude goes out to the members of Dr. Harris' research group for their free yet invaluable help and encouragement. Last but not least, to my wife Camesia, and my sisters, Jermella and Jonelle Matthews, for giving me unconditional and invaluable emotional support.

TABLE OF CONTENTS

LIST OF TABLES

LIST OF FIGURES

1. INTRODUCTION

Silica, (or SiO_2), a compound of silicon, is one of the most abundant compounds, accounting for 78% of the earth's crust. Silica is particularly important for industrial applications in which it is frequently exploited for its porosity and high surface area. Iller (1979) reports that silica particles in an acidic solution (pH<7) or in a salt solution of pH 7-10, aggregate into three-dimensional networks and form gels. The three important physical characteristics of colloidal gels are the size and shape of the primary particles, the spatial distribution of the particles, and the strength of the bonds between particles. These characteristics can be controlled to some degree by the method of preparation (i.e. temperature and concentration). The porosity and surface area are, in turn, dependent on these characteristics.

Silica gel particles have fast become an important fixture in today's technology. From the micron-sized gels used as adsorbents in HPLC columns to the moisture absorbing beads of a silica gel packet found in a brand new shoebox, their usage extends to numerous applications. Silica gel particles are also a very good base for catalytic additives. It is even the preferred choice for many optical systems (Hench 1998).

Although the inherent chemical nature of silica (adsorbtivity, inert, high melting point etc.) is a key advantage to the applicability of silica gel particles, a lot of their functionality lies in the control of particle size and

morphology. Some aspects that are affected by size and morphology include porosity, density, surface area and optical and acoustical transport properties. Specific surface area (the surface area per unit mass), in particular, is a key factor in commercial applications simply because the surface is the active site for most applications. High specific surface area is defined as being on the order of 100 m^2/g or greater (Otterstedt and Brandreth 1998).

There are many processes for producing gel particles. Iller (1979) gives examples of a few of these. One method involves grinding or pulverizing bulk gels into a powder. This process is simple, but presents very low control on the shape of the particle.

Particles can be formed under certain drying and freezing conditions with subsequent cracking to form particles. This family of techniques is also a poor method of forming particles of spherical geometry. Spherical particles are usually desired because they have a well defined symmetry suitable for coating, packing and mathematical analysis, among other things.

One spray technique, called emulsion polymerization, is the dispersion of droplets of acidified silicate into an immiscible liquid where gelation occurs. It is a good method for forming spherical particles, but introduces the environmental problem of disposing the continuous phase, (usually an organic liquid) where emulsification takes place. Therefore, it is best to disperse the silicate solution into a more environmentally-benign

continuous phase fluid. Table 1.1 presents a comprehensive listing of some of the other principal spray methods leading to droplet/particle formation.

Table 1.1. Methods of Droplet Formation Used in Sol-Gel Processes (Wedlock 1994)

Method	**Size range**	**Comments**
Spray drying	$\approx$2-50 μm	Size control depends on spray formation and sol rheology (particles polydispersed)
Nozzle (gravity)	$\approx$0.5 to 2-3 mm	Monodispersed particles. Size depends on orifice diameter and sol rheology
Nozzle (spinarette – high-frequency vibration)	$\approx$50 μm to 0.5 mm	Monosized particles. Control depends on orifice diameter and vibration frequency
Water/oil emulsion	$\geq$0.5 μm to $\leq$30 μm	Good size control. Depends on water/oil interfacial tension, stirring rate and surfactant addition

This research aims to develop and investigate a process that produces high surface area silica particles by the atomization of acidified aqueous sodium silicate (also called waterglass) solutions, gelation of the droplets in air, and the subsequent drying of the particles in a heated collection chamber. The process requires no liquid in which to collect and

further process the particles, which is an environmental benefit. The focus of this study is to identify the key factors in this process that uses an ultrasonic spray nozzle to atomize the silica into fine droplets. The key factors that are monitored in this spray process are average volumetric flow rate through the nozzle, concentration of sodium silicate, and temperature of the collection chamber. Analysis of the affect of these factors on the particle size distribution and the surface area will be presented.

2. LITERATURE SURVEY

There is an extensive array of techniques in industry for producing gel particles or ceramic powders. In addition, research laboratories are incessantly attempting to come up with new or improved techniques that aim to increase the specific surface area, reduce production cost, or produce more geometrically uniform particles. The central process pursued in this research combines features from previous techniques and presents some novel design features, which will be introduced in the Experimental Methodology chapter. In this chapter, some background will be given on the most popular techniques and their positive and negative aspects.

2.1. Comminution

Pulverizing bulk gel to form smaller particles is the oldest and most primitive technique employed in forming ceramic powders or gel particles. The term used to describe the reduction of large-sized solids into smaller ones by mechanical methods is known as “comminution” (Ganguli and Chatterjee 1997). Some examples of comminution are grinding, crushing, and milling. Crushing produces particles in the size range of approximately 1 mm. This is beyond the size range of many technological applications, including chromatography column packing and surface coating applications. Grinding and milling are synonymous in that most mills employ the use of a grinding media for the particle breakup. Mills produce

fine powders by proceeding through the mechanisms of compression, mechanical impact, and/or particle attrition or particle wear at high velocities (Ganguli and Chatterjee 1997).

The roller mill utilizes the mechanism of compression to further reduce previously crushed material. The coarse material is passed through two rollers which impose mechanical stress on the bulk material, thereby producing powder. Mechanical impact of a different sort is performed in the other more popular mills such as the ball mill. The mill (or chamber) is filled with feedstock, hard ceramic or metal grinding media, and sometimes water. The mill is rotated and interaction between the grinding media and the feed material occurs. A more specialized type of grinding mill is the attrition mill, or attritor. In this design, the chamber is stationary, but encloses a rotating stirrer system that more effectively induces the interaction between feed and grinding material. This technique can produce particles as small as 0.1 microns, while the other mills usually produce 1-20 micron particles.

Much discussion can be presented on the different types of comminution techniques, but their pros and cons are relatively similar. They produce fine particles, whether the feedstock is wet or dry, with uncomplicated processes. The limitations include contamination from wear of the grinding media, additional unit operations such as separation and drying, and high energy input to provide the mechanical power or to cool

the system. Even more so, there is absolutely no control over the shape or morphology of the particle, if this is desired.

2.2. Surfactant Templating

Surfactant templating is one of the more recent developments in the synthesis of particles. The general aim of this method is to exploit the bi-polar nature of surfactant molecules in solution with hydrolyzing silicate. The particle formation mechanism is the encapsulation of precipitating silica (or other) particles and subsequent formation of the desired spherical particles upon washing, air drying, and heating to remove the surfactants (Qi et al. 1998). The encapsulating structure is known as a "micelle" and is formed when the concentration of surfactant in solution reaches the critical micelle concentration (CMC) and the surfactant molecules associate to form a definite structure of a hydrophobic core and a hydrophilic surface, if the solution is aqueous (Hiemenz and Rajagopalan 1997).

Ionic (Kresge, Leonowicz et al. 1992) and neutral (Tanev and Pinnavaia 1995) surfactants have been used as templates, but the results were agglomerates with particles of a wide size distribution. Qi et. al (1998) report that mesoporous silica spheres ranging from 2 to 6 μm in size can be produced in static (not stirring the solution) acidic conditions using mixed cationic-nonionic surfactants as the template. The time of this synthesis is 16 hours. However, for liquid phase chromatography techniques and fluidized-bed catalysis applications, spheres with larger

sizes (while remaining less than 1 mm) are required. (Kosuge and Singh 2001) describe a technique to synthesize Al-containing silica particles in 80 minutes using 1-alkylamine as the templating surfactant in stirred acidic conditions. Their study concluded that octylamine templating produces mesoporous particles of 30-50 μm mean diameter and specific surface areas of 800 m^2/g at 600 ^0C.

The control of particle morphology and size comes at no small cost for surfactant templating techniques. The number of components involved limits the range of reacting conditions, and with both techniques, very high temperatures were required to remove the surfactant.

2.3. Emulsion Polymerization

This technique is quite similar to the previous method in that it utilizes the process of encapsulation. In emulsions, encapsulation occurs when a mechanical disturbance overcomes the immiscibility of two liquids (Hiemenz and Rajagopalan 1997). For the case in which water is encapsulated by oil, the water is called the “dispersed” phase and the oil is called the “continuous phase”. For the problem of particle synthesis, emulsions are basically used as micro-reactors for the particular silica formation reaction. The difference from the previous technique is thatthe morphology of the emulsion itself is formed by other means, and then the particle is produced within the emulsion and consequently takes on its shape.

The free energy required to form droplets from two immiscible liquids is proportional to the interfacial tension between the liquids (Wedlock 1994):

$$\Delta G = \gamma \Delta A, \qquad (2.1)$$

where γ is the interfacial tension and ΔA is the change in surface area. The mechanical energy required to form emulsion droplets is inversely proportional to droplet size and becomes very large to form colloidal size droplets (Wedlock 1994). Comminution methods such as mills, mixers, and high-pressure homogenizers are used to form emulsions, at an expensive energy cost (Lissant 1983). In many cases, surfactants are used to reduce this energy requirement by reducing the surface tension between the two phases by about 25-50 mN m^{-1} (Hiemenz and Rajagopalan 1997).

2.4. Electrodispersion

A relatively new technique that uses an electrical field to disperse the aqueous phase into the organic phase has gained interest. This technique is referred to as "electrodispersion". It requires considerably less energy because electrical stress occurs at the liquid-liquid interface where there is a large difference in the dielectric properties of the disperse/aqueous phase ($\varepsilon > 70$) and the continuous/organic phase ($\varepsilon < 10$) (Harris, Scott et al. 1993). Electric fields atomize the aqueous phase, which contains the metal salt solution (i.e. sodium silicate) into the oil phase, which contains a

precipitating agent (i.e. acetic acid). This atomization forms the emulsion micro-reactors and provides the locale for the condensation/precipitation reaction and the framework for the resulting particle morphology. Terry (2001) reports a study of precipitating sodium silicate with acetic acid and the formation of rigid gel spheres of about 20 μm in diameter. The particles also resistagglomeration and clustering. The generation of organic waste and the added washing steps tied to this method are its unwanted features.

2.5. Ultrasonic Atomization

Ultrasonic atomization uses ultrasonic waves to break up a bulk liquid into droplets. An ultrasonic nozzle operates at a specific resonant frequency that is determined primarily by the length of the nozzle (Berger 1998). The frequency is also the primary factor affecting droplet size, but other factors affecting mean droplet size are liquid viscosity, the tension at the liquid-air interface, nozzle orifice diameter and the flow velocity. This method has been utilized mainly in aerosol systems that produce porous silica powders of 1–3 μm (Amiel, Heintz et al. 1990) or as small as .3 μm (Aegerter et al., 1989). The combination of electrical and mechanical power in this process introduces the benefit of being more energy efficient than the previous techniques.

A technique that follows the precipitation reaction of the electrodispersion technique, without the generation of large amounts of

liquid waste, and employs the power of ultrasonic atomization, is the goal of the current research.

3. EXPERIMENTAL METHODOLOGY

The chief objective of this project is the design of the reactor system to produce silica particles by ultrasonic atomization. Tightly coupled with this objective is the subsequent analysis of the silica particles by appropriate tools and techniques to measure the responses – specific surface area and particle size. In designing the Acoustodispersion Precipitation Reactor(APR), it is also necessary to carry out preliminary experiments to determine the limits of the experimental levels for the three factors – sodium silicate concentration, chamber temperature, and flow rate through the nozzle. This section outlines in detail, the procedures followed in performing the preliminary experiments, designing the APR, and collecting and preparing the particles for SEM (scanning electron microscopy) imaging and employing a gas sorption apparatus for surface area analysis. The chemicals, materials, and equipments used will also be introduced in the presentation of each section.

3.1. Overall Reaction Scheme

The general procedure is as follows:

Two pumps, which are each equipped with a power supply/variable controller, are set to provide equivalent flow rates of sodium silicate and sulfuric acid to a cylindrical mixer. The mixing chamber sits on a Fisher magnetic stirrer and inside the mixer is a magnetic stir bar. Valves are

positioned in appropriate locations so as to avoid back-flow and contamination in the separate lines. After the two components are mixed, the gelling solution is pumped to the ultrasonic nozzle, where it is atomized into a fine mist and falls through a heated chamber (dryer), which is heated by a heat gun, and into a rectangular basin. Particles are collected after two minutes. A diagram illustrating the process is shown in Figure 3.1.

3.2. Gelation Time Experiments

A brief theory of the gelation of sodium silicate is presented to supplement the explanation of the preliminary experiment needed to determine the operating limits based on silicate concentration.

3.2.1. Theory of Gelation

The primary reaction is the gelation of sodium silicate. In general, the formation of gel results from an ion exchange of Na+ for H+ in a sodium silicate solution (Gerber, Himmel et al. 1994), causing the primary particles to aggregate (see equations 3.1-3.4). The formation of gel can follow one of two pathways. The first most common pathway is that where the pH is above the iso-electric point (pH = 2 for sodium silicate). Above this point the reaction is OH^- catalyzed (Gerber and Knoblich 2001). The gel formation rate is at a minimum at the iso-electric point and increases until the point (pH = 6).

Figure 3.1. Diagram of the Acoustodispersion Reactor (APR)

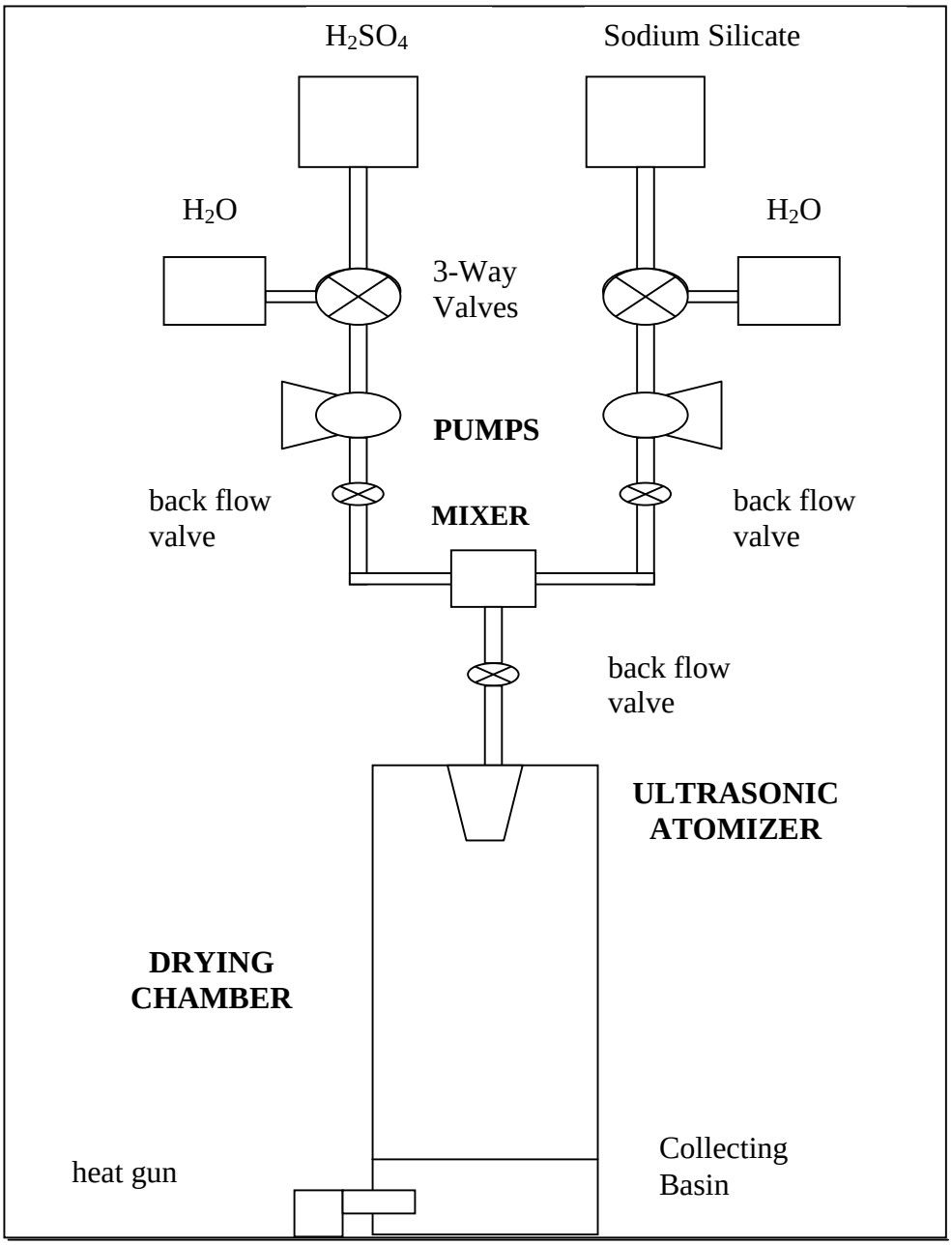

Above pH 6, electrostatic repulsion and other factors limit aggregation and slow gel formation. This OH- catalyzed phenomenon exhibits the following mechanism (Gerber and Knoblich 2001):

$$Na^+ + \text{-SiOH} + OH^- \rightarrow \text{-SiO}^- + H_2O \quad (3.1)$$

$$\text{-SiOH} + \text{-SiO}^- \rightarrow \text{-Si-O-Si-} + OH^- \quad (3.2)$$

Below the iso-electric point, a different mechanism occurs, where the silicate solution is proton catalyzed and follows a proton stabilized intermediate which then decomposes (Gerber and Knoblich 2001).

$$\text{-SiOH} + \text{-SiOH} \ldots H^+ \rightarrow [\text{SiOH} \ldots \text{SiOH}_2]^+ \quad (3.3)$$

$$[\text{SiOH} \ldots \text{SiOH}_2]^+ \rightarrow \text{-Si-O-Si-} + H_2O + H^+ \quad (3.4)$$

For the case of sulfuric acid as the precipitating agent, sodium sulfate will precipitate as a by-product of this reaction. The proton catalyzed mechanism is employed in this project because the pH of the acidified sodium silicate ranges from 2 – 6 (based on the concentrations of acid used to achieve the required gelation time).

A stock solution of 6.3 mol/L (M) of aqueous sodium silicate (mole ratio of 3.36 SiO_2: Na_2O, 27.4 wt. % SiO_2) was obtained from W.R. Grace & Company. The acid that was used to induce gelation is reagent grade sulfuric acid (~18 N) from Aldrich Chemicals, Inc. These, along with

distilled water (H_2O) as a diluting agent, were the sole chemicals used in the particle synthesis.

3.2.2. Gelation Time Measurements

In order to determine the concentration (or pH) of sulfuric acid that induces gelation for the specified levels of silicate concentration, a series of batch gelation experiments were carried out. The three levels of concentration of sodium silicate were made by dilution with water. The stock solution was diluted to 45%, 55%, and 65%, corresponding to 2.88 M, 3.52 M, and 4.16 M respectively. Equal volumes of the acid and sodium silicate were dispensed with a micro-pipette into a 5-ml glass vial, hence the term, “batch”. The vial was quickly shaken and then slowly tilted from side to side until the gelation time was reached (when the meniscus no longer reverted to its original position upon tilting). Results are presented in chapter 5.

3.3. The Acoustodispersion Reactor

The Acoustodispersion Precipitation Reactor consists of four major unit operations – pumping, mixing, atomization, and drying. This section describes each operation in detail. The equipment and materials used to perform each unit operation are listed in a table, followed by the procedure.

3.3.1. Pumping

Table 3.1. Equipment and Materials for the Pumping Unit Operation

Quantity	**Equipment**	**Make**	**Model**
2	Pump head	Micropump	P-07002-33
2	Pump drive	Micropump	P-07002-39
2	DC Power Supply/Speed Controller	Cole-Parmer	P-02630-85

All the parts of the pumping unit were obtained from the Cole-Parmer Instrument Company. The purpose of the pumping unit was to deliver sodium silicate and sulfuric acid in equal quantities to the mixer, atomizer, and finally to the collecting chamber. The pump heads used were pressure-loaded gear pumps.

The inlet sides of the pump lines ran from the feed solutions of sodium silicate and sulfuric acid. The sodium silicate was contained in a Nalgene (plastic) beaker and the sulfuric acid was placed inside a glass beaker. Three-way valves were strategically placed between the feed solutions and the pumps. The second input into these valves was a beaker of tap water, which was used to flush the system after every run. The lines from the outlet ran from the pump to the mixer.

The DC power supply had to be calibrated to determine the corresponding flow rate for each setting. Tap water was conveyed through one pump to a beaker sitting on an electronic balance. After one minute, the mass of the water, calculated from the density ρ=0.99821 g/cm^3 at 20 ^{0}C (CRC Handbook of Chemistry and Physics, 2000) was recorded. The settings ranged from 1 to 10 and triplicate readings were taken at settings 1 through 6 and at setting 9. The experimental design settings are 4, 5, and 6. The flow rates that these settings correspond to are presented in the results chapter. Random testing was also done at different settings to confirm that the flow rate was additive upon exiting the mixer. The results are reported in the Results and Discussion chapters.

3.3.2. Mixing

Table 3.2. Equipment and Materials for the Mixing Unit Operation

Quantity	**Equipment**	**Make**	**Model**
1	Cylindrical Mixing Chamber	Designed by Professor Michael Harris and Edd Cole	---
1	Magnetic Stir bar	Fisher Scientific	n/a
1	Magnetic stirrer	Fisher Scientific	n/a

The mixing process initiated the gelation reaction. Stop-flow valves were placed between the mixing unit and the pumps so as to maintain the

integrity of the feed solutions and to prevent the pump from being subjected to abrasive particulates.

The mixer (see Figure 3.2) was specially designed at the University of Maryland in the experimental workshop of the Institute for Physical Science and Technology. The mixer is a 20-ml plexiglass cylinder (6.5-cm in diameter, 3-cm height) with two inlets and one outlet, all of 1 mm inside diameter. The two inlets were placed at the top of the nozzle and the outlet was placed at the bottom. The magnetic stirrer inside operates at a speed of 1200 rpm. The top is removable which allows for cleaning of the chamber and magnetic stirrer. Following the mixer is another stop-flow valve which was placed to maintain the integrity of the mixed solution.

The results of the gelation experiments coupled with the knowledge of the flow rate, helped to determine a mixing length (or the length between the mixer and the atomizer) suitable for the pre-determined gelation time of 60 seconds.

Figure 3.2. Schematic of the Mixing Chamber

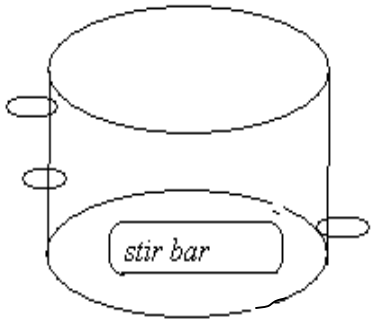

3.3.3. Atomization

At the very heart of the APR system is the ultrasonic nozzle used for atomization of the gelling solution. Table 3.3 lists the specifications for the particular ultrasonic nozzle that we used.

Table 3.3. Specifications for the Lechler US 1 Ultrasonic Nozzle

Company	Lechler Company, Germany
Model	US 1
Atomizing Frequency	100 kHz
Most frequent drop diameter	20 μm
flow rate range	1 - 25 mL/min
Chamber diameter	38.1 mm
Orifice diameter	0.5 mm

The fluid entered the inlet and contacted the atomizing surface, which was vibrating at a frequency of 100 kHz. The mechanical energy from the vibration rips the liquid into small droplets that are then forced through the atomizing horn in a conical spray pattern. A correlation for droplet diameter (d_d) as a function of frequency (f) is (Berger 1998):

$$d_d = 0.34 (8\pi s/\rho f^2)^{1/3} \quad (3.5)$$

where s is the surface tension and ρ is the density.

Figure 3.3 below shows the major working parts of a typical ultrasonic nozzle.

Figure 3.3. Basic Outline of an Ultrasonic Nozzle with its Working Parts

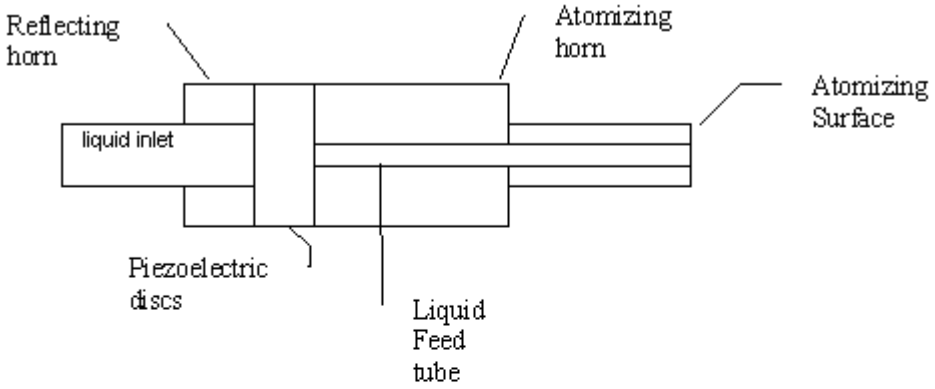

3.3.4. Drying

Table 3.4. Equipment and Materials for the Drying Unit Operation

Quantity	**Equipment**	**Make**	**Model**
1	Drying Chamber	Modification of existing chamber by J.N.A. Matthews and Edd Cole	---
1	Heat Gun	Milwaukee	2000D
1	Mercury Thermometer	Fisher Scientific	15-000C

The final unit operation before collection for analysis is drying. As was previously mentioned, the ultrasonic nozzle receives the gelling fluid and atomizes the fluid into droplets. The spray was collected in a drying chamber modified from a previous design by M.T. Harris (see figure 3.4) whose cross sectional area was large enough to avoid the conical spray pattern contacting the walls, and high enough that the droplets would dry before they hit the bottom. The chamber was made of fiberglass and it was 1.52 m high and the square cross sectional area was 0.3 m^2. A 0.038 meter in diameter hole was placed at the removable top, and was used to center the nozzle in the drying chamber. The bottom of the chamber was also made to be detached in order to collect the particles. This detachable "collecting" bin was 0.1 m high. A heat source was inserted in a 0.038 m hole in the side of the chamber to accommodate the heat source. The

heating source was a heat gun that had a temperature range of 52 ^{0}C – 542 ^{0}C and settings from 1 to 10. The heat gun was calibrated and the results are presented in the results chapter. A mercury thermometerthat ranged from -1 ^{0}C to 201 ^{0}C (+/- 0.1 ^{0}C) was taped 0.076 m above the collecting bin on the opposite side of the heat gun. The collecting bin was lined with foil and the particles were washed off the foil and into a vial for further analysis.

Figure 3.4. Schematic of the drying system (drawn by Patrick Taylor)

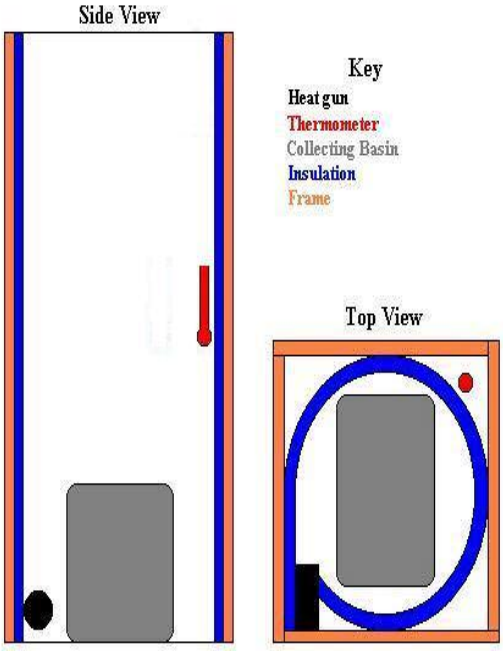

3.4. Analysis/Characterization

The particles were all collected and stored in distilled water and/or ethanol. After each vial was appropriately labeled, the next step was to study the particle morphology and find the particle size and the specific surface area, which were performed by SEM analysis and by nitrogen adsorption multi-point BET (Brunauer, Emmett & Teller) analysis, respectively.

3.4.1. SEM Analysis

The particles were placed on a carbon coated stud and were dried in an oven at 50^0C for ten minutes. The studs were then sputter coated with gold to provide better resolution during imaging. Imaging was carried out at 15 kV on a Scanning Electron Microscope (Amray 1820D) and images were taken from different areas of the stud and at different magnifications.

3.4.2. BET Analysis

BET surface area analysis requires the particles to be very dry. The first step was to dry the particles in the sample cell that was to be used in the Quantachrome NOVA 1200 Particle Analyzer. The procedure for determination of the specific surface area was as follows:

1. Sample was placed inside the sample cell and dried at approximately110^0C for 1 hour.
2. The mass of the sample was determined on an electronic balance.

3. The sample was degassed at 110^0C for approximately 2 hours by the Nova 1200.
4. The sample was re-massed to see if sample was lost.
5. The sample cell was then connected to the NOVA 1200 instrument and 6 point BET analysis is performed (see Appendix A for the BET Equation).

4. STATISTICAL OVERVIEW

The systematic method of experimentation which allows for greater ease and accuracy of data analysis was employed in this research. This process is simply known as 'design of experiments', or DOE for short. The reaction system in this research involves 3 factors/independent variables at 3 levels/points and 2 responses/dependent variables. The process of choosing a method or design that efficiently sets the number of replications to run for each combination of factors while maintaining statistical accuracy is the topic of this chapter. Using a statistical DOE software package, *Design-Expert 6.0.4 (Anderson and Whitcomb 1999),* the order of runs and analysis was chosen and a mathematical model was developed using a finely tailored regression analysis fit for the selected design choice.

4.1. Choosing an Appropriate Statistical Design

There are many design choices for experimentation, and care must be taken in choosing the most appropriate design. The main objective of the foregoing research was to derive a mathematical model for the specific surface area as a function of three factors and their interactions at three different levels. It has been decided that the temperature of the collecting chamber, the volumetric flow rate of the mixture, and the concentration of sodium silicate, were the factors to be studied. Their effect on the responses of interest, particle size and specific surface area, will be studied. To

summarize, the design consists of three quantitative factors at three levels and two responses. Since the experiments involve more than one factor, the response(s) will be represented by a surface. Therefore, the design family of choice is RSM, or Response Surface Methodology.

4.2. Response Surface Methodology

Response surface methodology is defined as "…a collection of statistical and mathematical techniques useful for developing, improving, and optimizing processes" (Myers and Montgomery 1995). Myers and Montgomery go on to report in the book, "Response Surface Methodology" that the method is a combination of design fundamentals, regression modeling, and basic optimization techniques. The goal is to approximate a measure of performance or response to independent variables or factors by using a first or higher order polynomial function originating from a Taylor approximation. The result is an equation and a graphical representation that is an approximation to the behavior of the process within the selected region of interest. The high and low levels of the factors bound the region of interest.

The general relationship is represented as such:

$$y = f(\xi_1, \xi_2, ..., \xi_k) + \varepsilon \tag{4.1}$$

The letter y is the response, ξ is the independent variable, f is an unknown function and ε is a term that represents variation not represented

in f, or random error. If ε is assumed to have a normal distribution with mean zero and variance σ^2, then the relationship takes on the form

$$E(y) = \eta = E[f(\xi_1, \xi_2, ..., \xi_k)] + E(\varepsilon) \quad (4.2)$$

where E represents the mean. Randomizing improves the assumption that the mean is equal to zero, which amounts to eliminating ε. The variance of random error term is the variation of the experimental point from the approximated point generated by the chosen model. A normal probability plot of the standardized residuals can be used to assess the plausibility that ε has a normal distribution (Devore 2000). More concerning the analysis of the model will be given in the Discussion chapter.

As mentioned earlier, the typical function of choice in regression analysis is the polynomial function. This is because a continuous function can be approximated by a polynomial and the approximation improves as the region of interest is narrowed or as the order of the polynomial increases.

The general first-order (or linear) model is

$$\eta = \beta_0 + \beta_1 x_1 + \beta_2 x_2 + ... + \beta_k x_k \quad (4.3)$$

and the second-order (or quadratic) model is

$$\eta = \beta_0 + \sum_{j=1}^{k} \beta_j x_j + \sum_{j=1}^{k} \beta_{ij} x_j^{\,2} + \sum \sum_{i<j} \beta_{ij} x_i x_j \quad (4.4)$$

where η is the dependent variable, x is the independent variable and β is its coefficient.

A first-order model is sometimes referred to as the main effects model (Myers and Montgomery 1995) because it contains only the effect of each variable on the response separately and does not give a true picture of how the variables affect each other, or interaction between the factors. Curvature or a "twist" in a response surface is an indication of interaction. Devore (2000) also states that the second-order polynomial is sufficient to describe the relationship for narrow factor ranges at which industry usually operates. Naturally, a quadratic model would be a better choice for application to this project. The two most popular designs that are capable of utilizing the quadratic model (as well as the lower level linear model) for Response Surface Modeling are the central composite (CCD) and the Box Behnken (BB) designs (Tranter 2000).

4.3. Comparing the Central Composite and the Box Behnken Designs

The central composite design is broken down into the CCF (central composite face-centered) and the CCC (circumscribed central composite). Table 4.1 is a comparison of the properties of these three designs.

Table 4.1. Comparisons of the Central Composite and Box-Behnken Designs

CCC	**CCF**	**BB**
No. of runs for 3 factors = 20	No. of runs for 3 factors = 20	No. of runs for 3 factors = 17
No. of levels for each factor = 5	No. of levels for each factor = 3	No. of levels for each factor = 3
Orthogonal blocks	No orthogonal blocks	Some have orthogonal blocks
Insensitive to outliers and missing data	Insensitive to outliers and missing data	Insensitive to outliers and missing data
Rotatable or nearly rotatable	Cuboidal rather than rotatable	Rotatable or nearly rotatable
Region of operability must be greater than region of interest	Region of operability and region of interest nearly the same.	Region of operability and region of interest nearly the same.

Some of these terms and their importance to this study must be discussed. The first term is orthogonality. Orthogonality says, "…different variable effects can be estimated independently. There is no correlation between the experimental levels of the independent variables. In the case of block orthogonality, it means that the effect of the blocks is independent of

the effects of the variables" (Kraber 2000). All three designs exhibit orthogonality, but only the CCC and BB designs allow for orthogonal blocks. For this research, no blocks will be utilized. Therefore this property is ineffectual.

Another term introduced is rotatablility. "Rotatability of a design implies that the variation in the response predicted by a model will be constant at a given distance from the center of the design" (Kraber 2000). Rotatability is a useful property that the CCC and BB designs both exhibit. The choice between the CCC and BB designs is made on the basis of cost and flexibility – the BB design employs three less experimental runs and it requires only three levels. In addition, the region of operability is neither known nor essential for this study because current interest is not geared toward predicting the response at the extremes. Therefore the choice is made to use the Box-Behnken design.

Table 4.2 represents the design layout for the 3-factor, 2-response BB design in coded format. The software automatically randomizes the run order. The low level is represented by –1, the high level by 1, and 0 represents the center point.

Table 4.2. Design layout for the Box-Behnken Design (courtesy of Stat-Ease, Inc.)

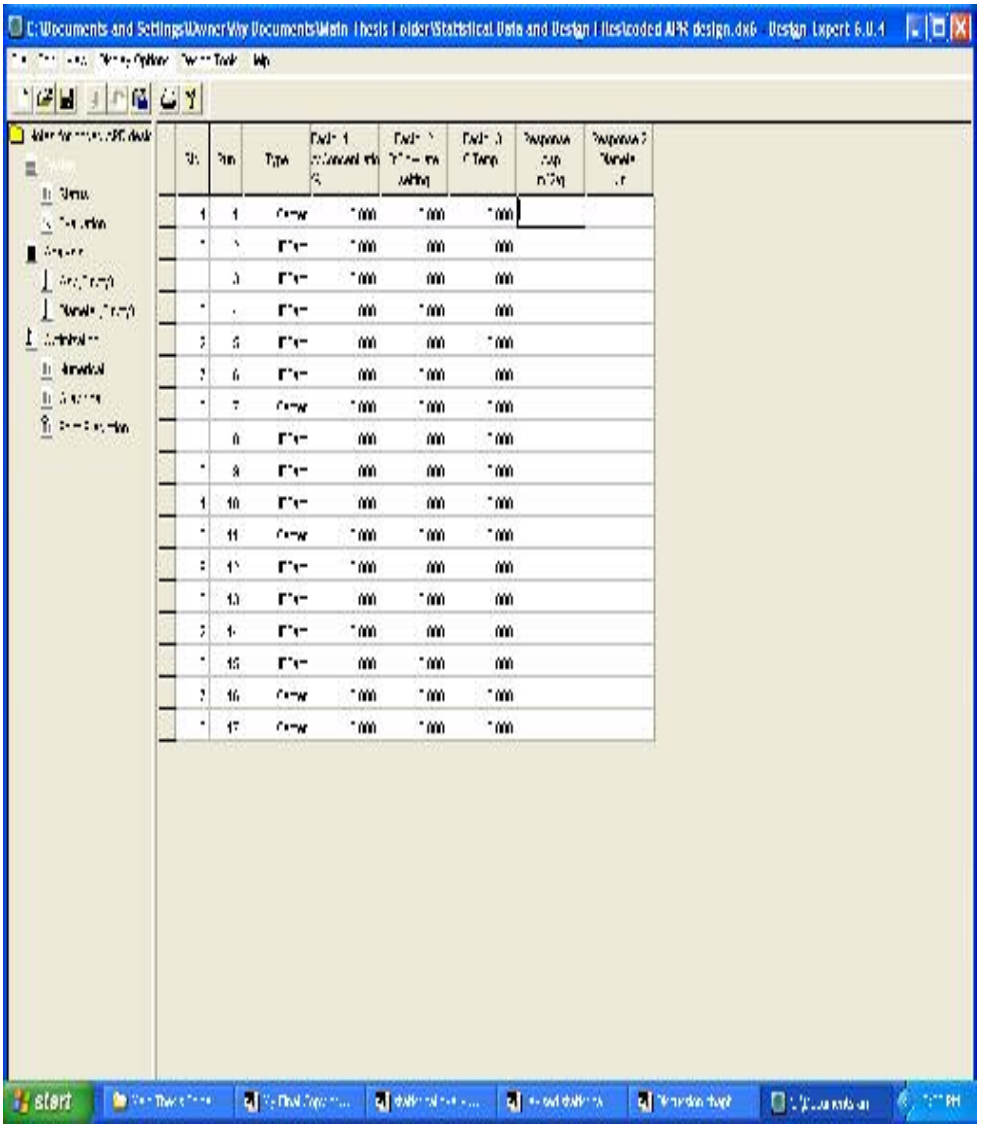

In this project the levels for concentration are sometimes given as a volume fraction, the flow rate is occasionally referred to by speed settings, and the true temperature in degrees Celsius is given. A concise description of these values is given in Table 4.3.

Table 4.3. Actual Values for the Coded Levels for the APR Experiment

Level	Factor	Value
-1	Concentration (M)	2.88
	Flow-rate (mL/min)	15
	Temperature (^{0}C)	50
0	Concentration (M)	3.52
	Flow-rate (mL/min)	20
	Temperature (^{0}C)	75
1	Concentration (M)	4.16
	Flow-rate (mL/min)	25
	Temperature (^{0}C)	100

5. RESULTS

There were three important pre-reaction experimental operations performed – pump system calibration, gelation time analysis, and drying system analysis. The two post-reaction analyses were SEM imaging/particle size analysis and BET specific surface area analysis. This chapter contains the presentation of data gathered in all these analyses in a tabular and graphical format.

5.1. Pump System/Flow-rate Calibration

In the scheme of the pumping system, the power supply/speed controller delivers the power to the variable-speed pump drive, which in turn controls to the pump head through which the pump lines run. Each of the two pump drives was capable of delivering a flow-rate of up to 20 mL/min. The speed controller was marked by even-spaced settings from 1 to 10, but did not come with a calibration curve. Consequently, a calibration curve had to be generated by experimentation in order to determine the flow-rate corresponding to each of the settings.

The pump system was set up to run through one pump. The pump line was then extended to a beaker sitting on an electronic balance and the mass of water delivered to the beaker in one minute was recorded. The mass was converted to volume using the density of 0.99821 g/cm^3 for

water. Triplicate runs were performed at various random settings and the results are presented in Figure 5.1 below.

Figure 5.1. Calibration Curve of Flow-rate Settings for a Single Pump

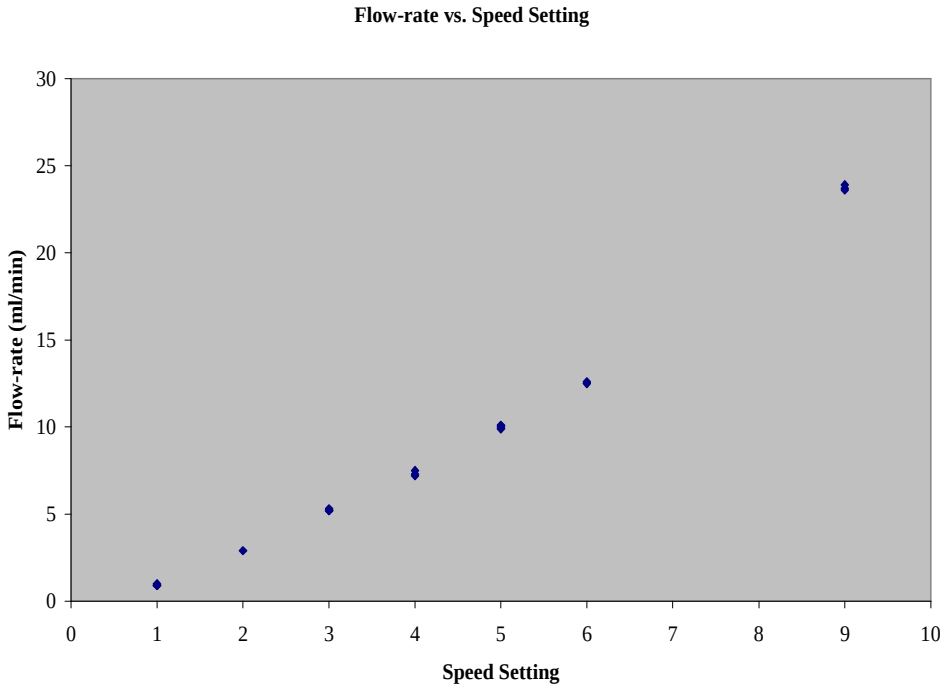

The trend exhibited in the plot seems to indicate that there is a non-linear increase of the flow-rate. Nevertheless, runs were performed at the experimental design settings of 4, 5 and 6 so there was no need to interpolate. These settings will be used in the experimental run and referred to by the setting number and not the actual flow-rate. The actual flow-rates for these settings are presented in Table 5.1 below.

Table 5.1. Actual Flow-Rate Corresponding to the Experimental Settings

Setting	Flow-rate (mL/min)	Avg. flow-rate (mL/min)	Combined flow-rate through nozzle (mL/min)
4	Run 1: 7.2 Run 2: 7.5 Run 3: 7.3	7.3 (+/- 1)	14.6 (+/- 1)
5	Run 1: 10.1 Run 2: 10.0 Run 3: 9.9	10.0 (+/- 1)	20.0 (+/- 1)
6	Run 1: 12.5 Run 2: 12.5 Run 3: 12.6	12.5 (+/- 1)	25 (+/- 1)

The experimental design flow-rates are therefore approximately, 15, 20, and 25 mL/min, corresponding to the speed settings of 4, 5, and 6. The mass flow rate of sodium silicate through the nozzle can thus be calculated, which can give the approximate mass of particles produced in two minutes. This information is presented in Table 5.2.

Table 5.2. Mass Flow-Rate and Grams of Particle Produced in Two Minutes Corresponding to the Specified Volumetric Flow-Rate and Concentration

Volumetric Flow-rate (mL/min)	15		20		25	
Molarity (mol/L)	**Mass flow rate (g/min)**	**Grams of particle produced (g)**	**Mass flow rate (g/min)**	**Grams of particle produced (g)**	**Mass flow rate (g/min)**	**Grams of particle produced (g)**
2.88	2.59	5.18	3.46	6.92	4.32	8.64
3.52	3.17	6.34	4.22	8.44	5.28	10.56
4.16	3.74	7.48	4.99	9.98	6.24	12.48

5.2. Gelation Time Analysis

The next phase of analysis before particle synthesis was the determination of thegelation time for the three experimental levels of the sodium silicate concentration. The gelation timeis hereafter defined as the time it takes the sodium silicate to gel completely. Gelation is catalyzed in this case by sulfuric acid.

Figure 5.2 shows the trend of the data obtained from the gelation time experiments. The estimates made for the concentration of sulfuric acid needed to produce a gelation time of 60 seconds are rough estimates. These estimates were chosen for the convenience and ease of preparation. The table for the gelation time data can be found in Appendix B.

Figure 5.2. Gelation Time vs. Concentration of Sulfuric Acid

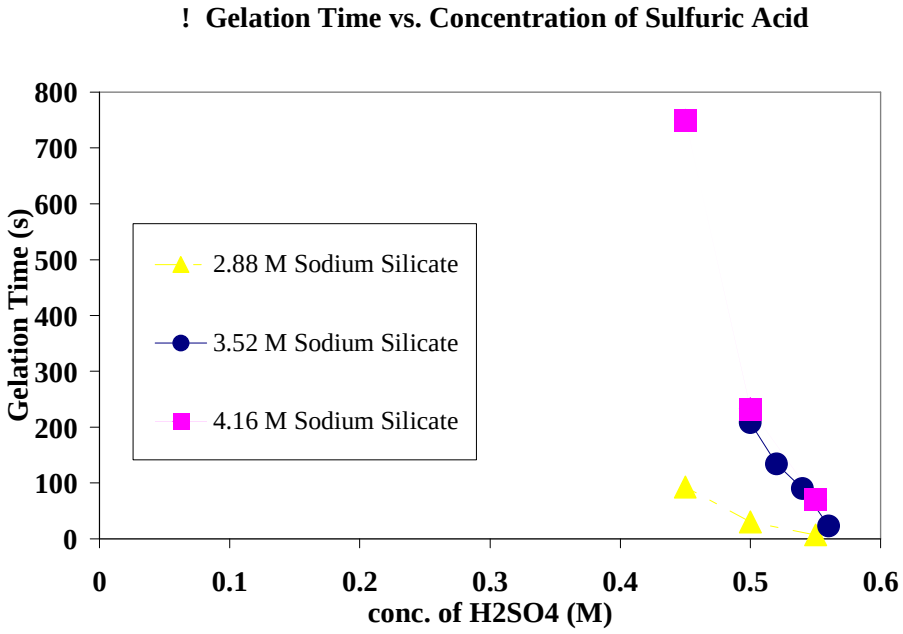

! *Indicated trendlines are shown only as a guide.*

5.3. Heat Gun Calibration and Drying System Analysis

The heat gun was used to control the temperature of the drying chamber. This Milwaukee brand heat gun is typically used for paint jobs and had a temperature range of 52 ^{0}C – 542 ^{0}C. The heat gun, like the speed controller for the pumps, also had dial settings from 1 to 10 and was not accompanied by a calibration curve. The object of the drying system analysis was to determine the time it takes the heat gun to raise the drying chamber temperature to the experimental points of 50 ^{0}C, 75 ^{0}C, and 100 ^{0}C at various settings. The results are produced in Table 5.3.

Table 5.3. Heating Time for the Drying Chamber

Level 5		**Level 9**		**Level 10**	
Time (s)	**Temperature (^{0}C)**	**Time (s)**	**Temperature (^{0}C)**	**Time (s)**	**Temperature (^{0}C)**
0.5	30	2	51	2	59
4.5	45	5	71	5	80
10	**50**	**6**	**75**	**10**	**97**
15	52	10	87	12	72
20	45	12	65	14	62

The results from the previous table show that it takes approximately10 minutes at level 5 for the drying chamber to heat up to 50 ^{0}C. It takes 6 minutes on level 9 for it to heat up to 75 ^{0}C, and 10 minutes on level 10 to heat up to approximately100 ^{0}C. The heat gun was removed after reaching the required temperature and the experiments were performed within the two minute time window before the temperature began to decrease.

5.4. SEM Analysis

Scanning Electron Microscopy was used to gain a perceptive of the morphology and the particle size. The particles were measured by a metric ruler (+/- 0.5 mm) and converted to the actual size after measuring the legend on the image. The results showed that the majority of the particles were rigid yet porous, spherical and most of them measured around 20 microns in diameter. A brief discussion of the morphology will be presented with the accompanying image.

Figure 5.3 are Samples 1 and 16, and they coincide with the center points of the design, where the values are at the middle levels. The SEM images of the other 3 center points are given in Appendix D. In this section and in some of the following sections, the samples will be occasionally be referred to by the coded level of their respective design points:

(C=concentration, Q=flow rate, T=temperature)

Figure 5.3. SEM Images of (a) Sample1 and (b) Sample 16, the Mid-Levels (0,0,0) of Each Factor

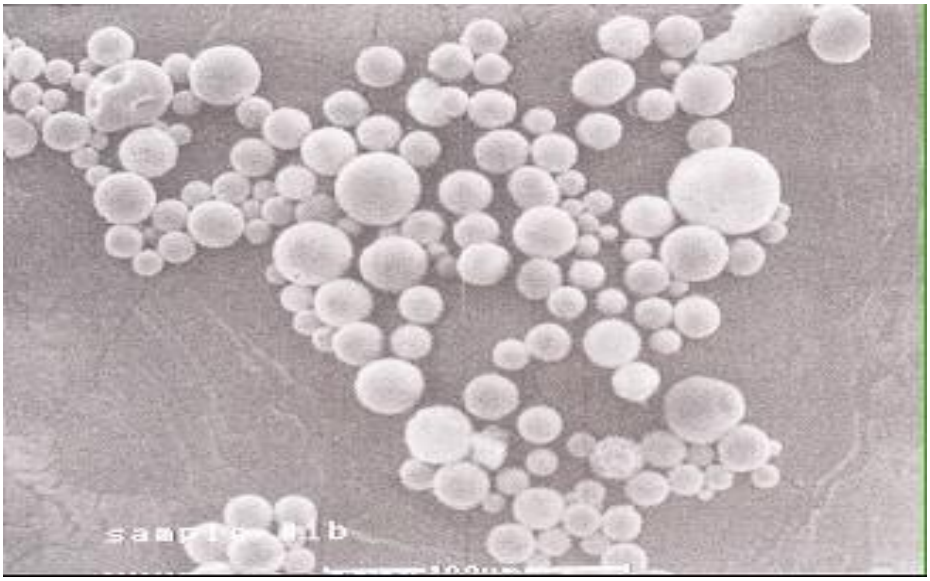

(a)

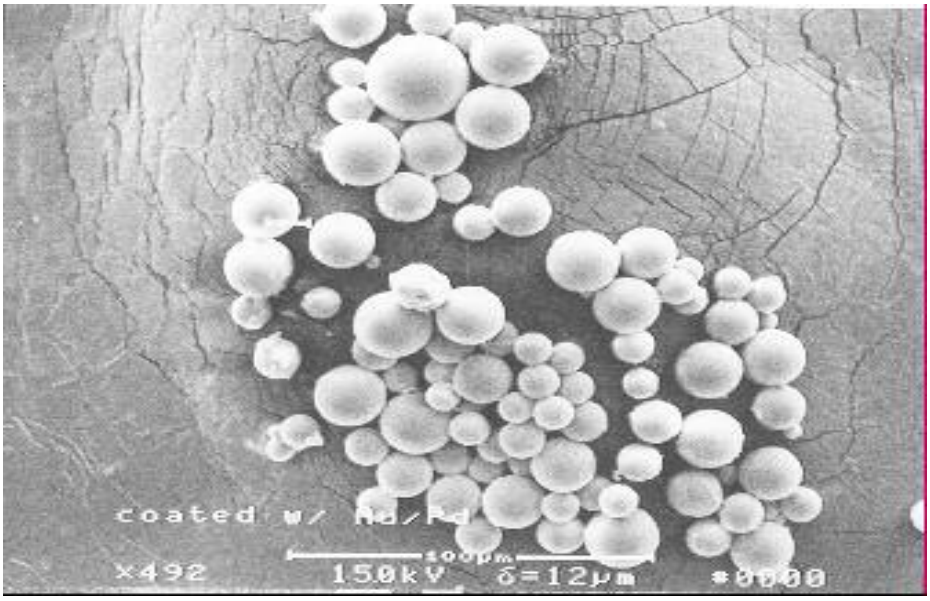

(b)

Sample 1 showsessentially spherical silica particles with very small number of exceptions. The particles are rigid and the population appears to be fairly polydisperse with the particle size ranging from 5 μm to 25 μm. The frequency distributions of all the center points are plotted in Figure 5.4. The number average diameter is around 20 μm.

Figure 5.4. Frequency Distribution of the Particles at the Center Points of the Experimental Design

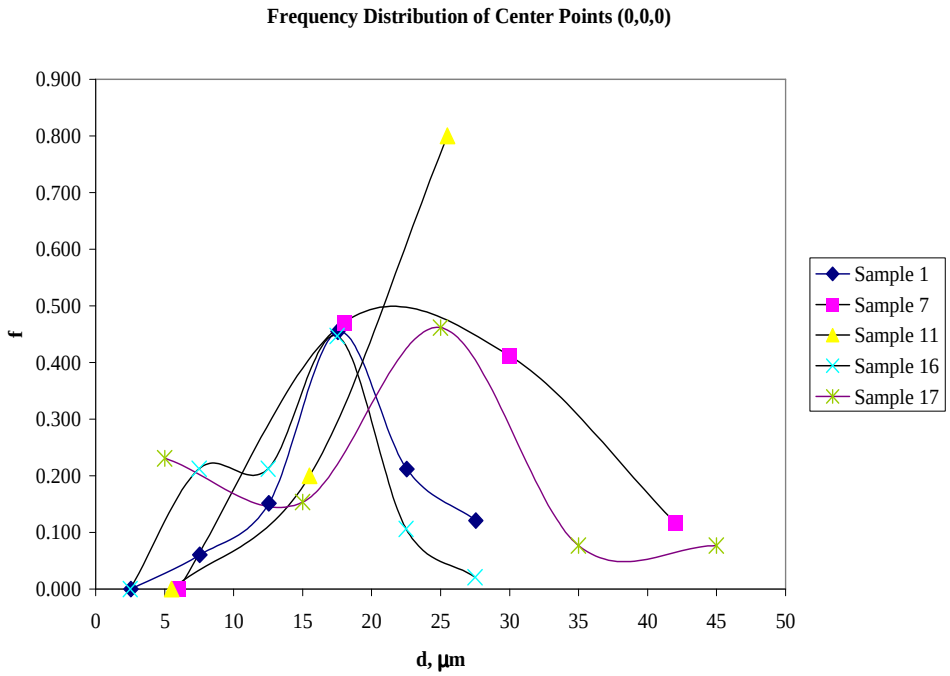

The images of Sample 2 and sample 6 showed inconclusive evidence of gel particles and are therefore not presented.

From this point, the presentation of the SEM images will proceed by run order, with some omissions made based on unhelpful evidence, and the remaining center point samples will be given in Appendix C.

Sample 3 was the point (0,-1, 1) – the middle value for concentration, the low value for flow rate, and the high value for

temperature. A few of the particles in the population appear rigid and spherical, but a significant number of them are oblong, cracked, or have indentations (see Figure 5.5).

Figure 5.5. SEM Image of Sample 3 (0,-1, 1)

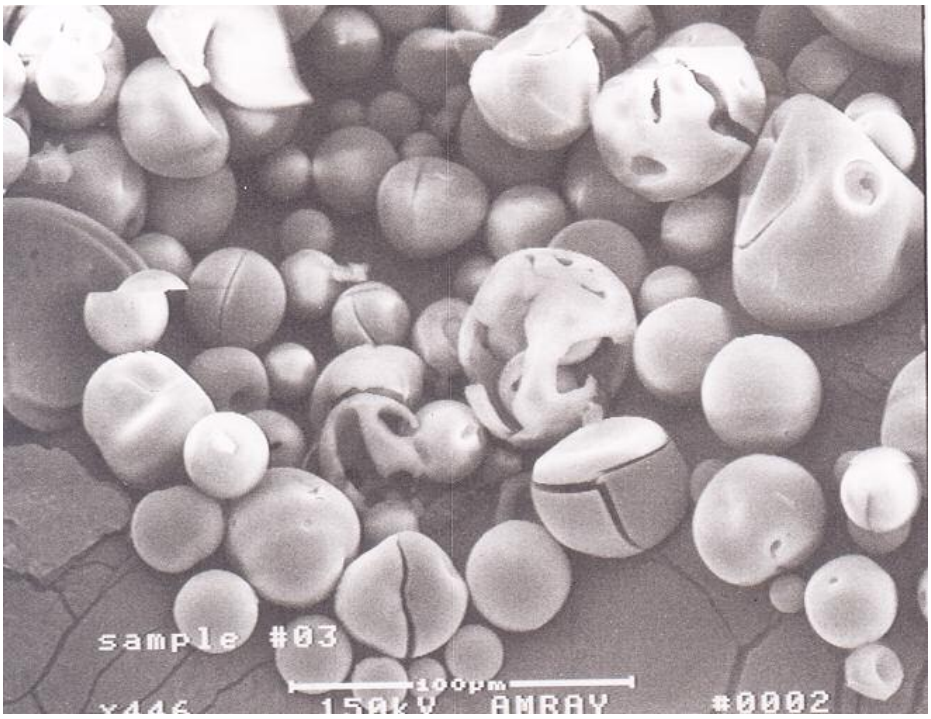

The image of Sample 4 (Figure 5.6) shows spherical particles embedded in a gel matrix. A marginal number of them are cracked and hollow.

Figure 5.6. SEM Image of Sample 4 (-1, 0,-1)

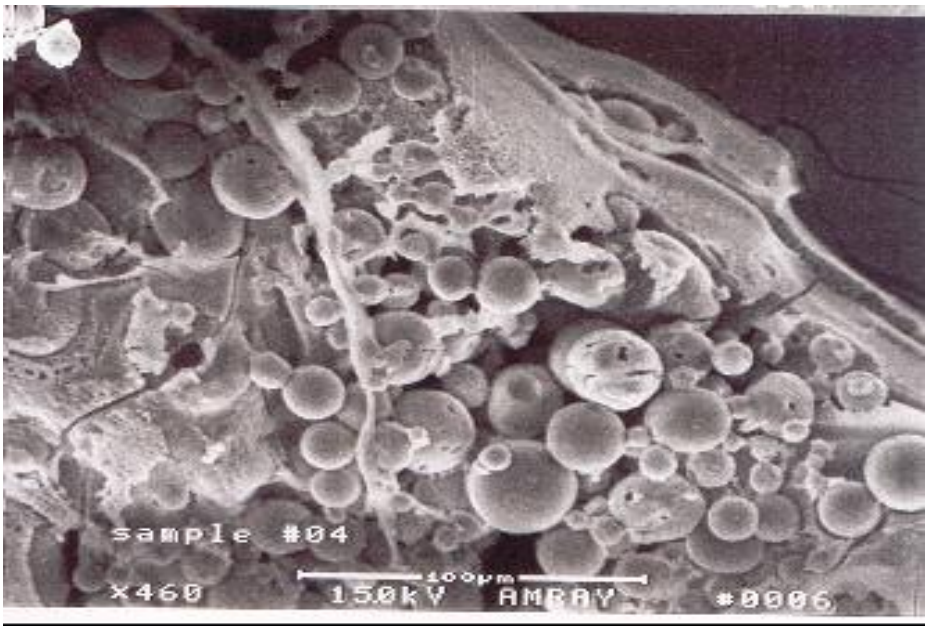

The image of Sample 5 (Figure 5.7) does not show many particles. What is pictured is a dusty, flaky gel clump covering about three large and spherical particles.

Figure 5.7. SEM Image of Sample 5 (1,-1, 0)

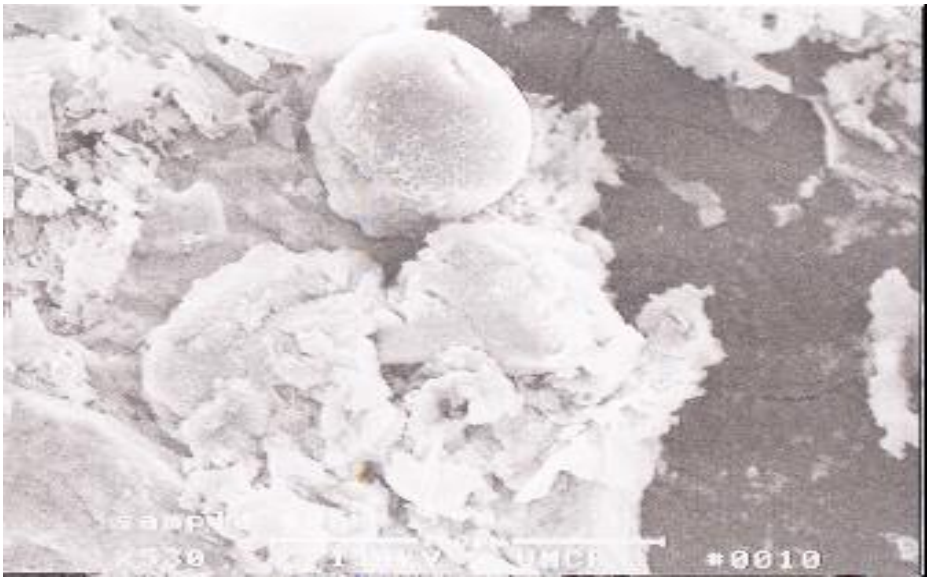

Sample 8 showed a large dimpled particle attached to a smaller spherical particle. The image only consisted of these two particles and is not presented.

Sample 9 corresponds to the point (-1, 1, 0). Figure 5.8 is the SEM image of sample 9 and it shows a large population of particles. Most of these particles are rigid and uniformly spherical. There are a few particles that are dimpled and oblong.

Figure 5.8. SEM Image of Sample 9 (-1, 1, 0)

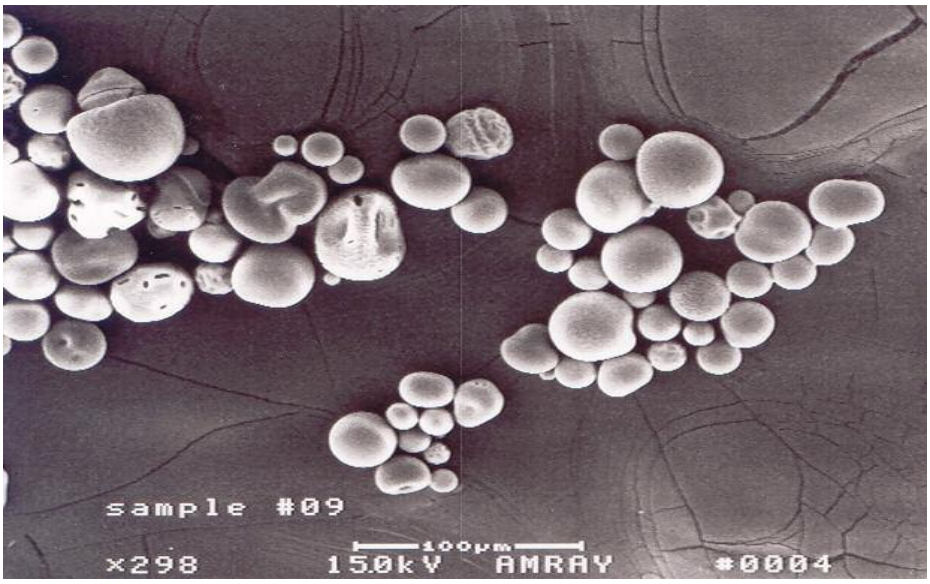

The particles pictured in Figure 5.9 are for Sample 10, point (1, 1, 0). The particles are rigid and are spherical and are located in a white powdery substance (probably silica gel). The particles are fairly mono-dispersed.

Figure 5.9. SEM Image of Sample 10 (1, 1, 0)

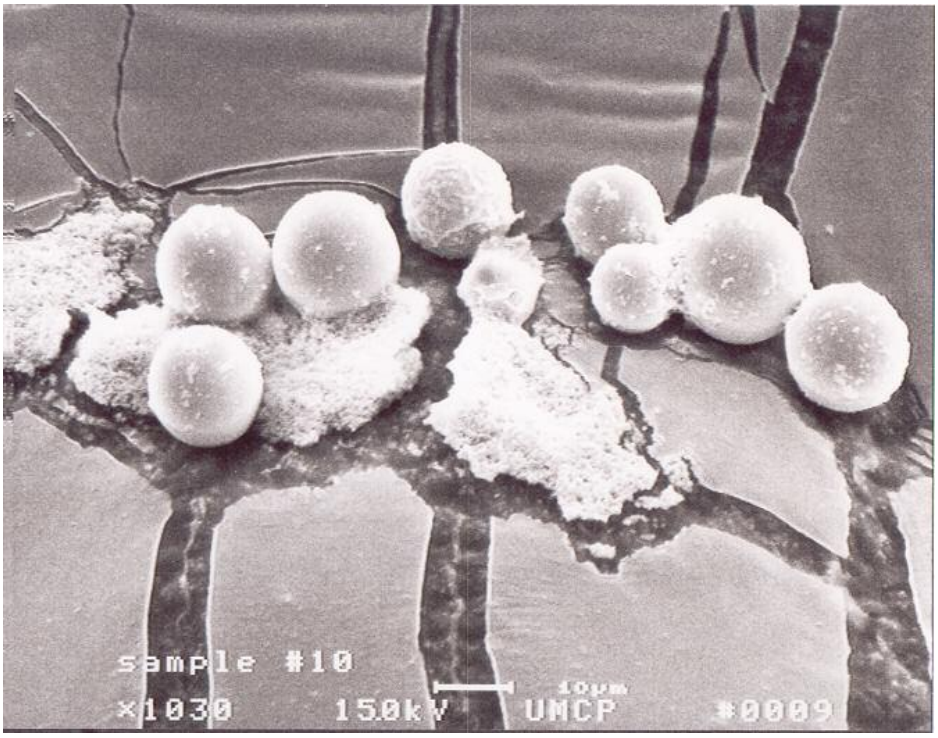

Most of the particles of Sample 12 (see Figure 5.10) are spherical. All of the images of this run, point (0, -1, -1), show the particles bunched closely together, probably by the glue from the carbon tape on the SEM stud.

Figure 5.10. SEM Image of Sample 12 (0,-1,-1)

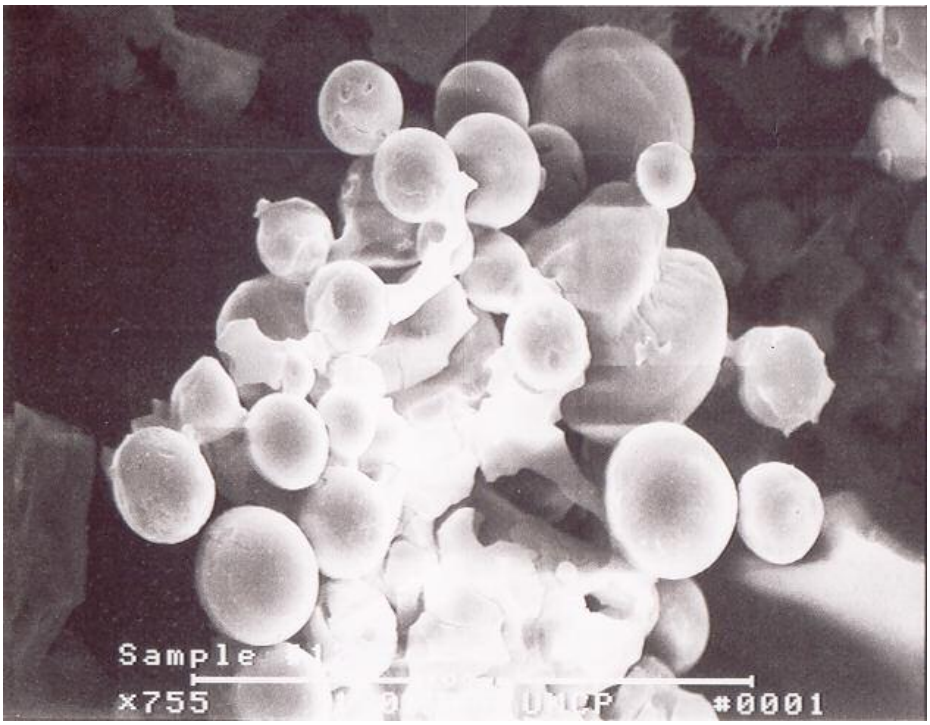

The image captured from Sample 13 (Figure 5.11) show some unusual phenomena. The particles, taken at point (1, 0, 1), have prickly exterior and one large particle is hollow, cut in half, and contains smaller, prickly particles.

Figure 5.11. SEM Image of Sample 13 (1, 0, 1)

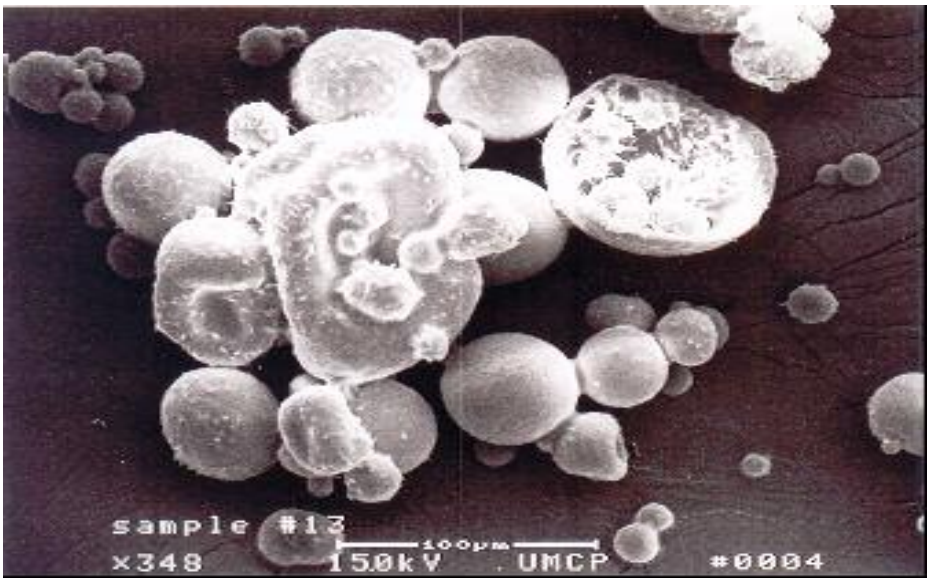

The image from Sample 14 (see Figure 5.12) shows some slightly warped but nearly spherical particles that are scattered across the stud. This is also at the same high level for temperature as sample 13.

Figure 5.12. SEM Image of Sample 14 (0, 1, 1)

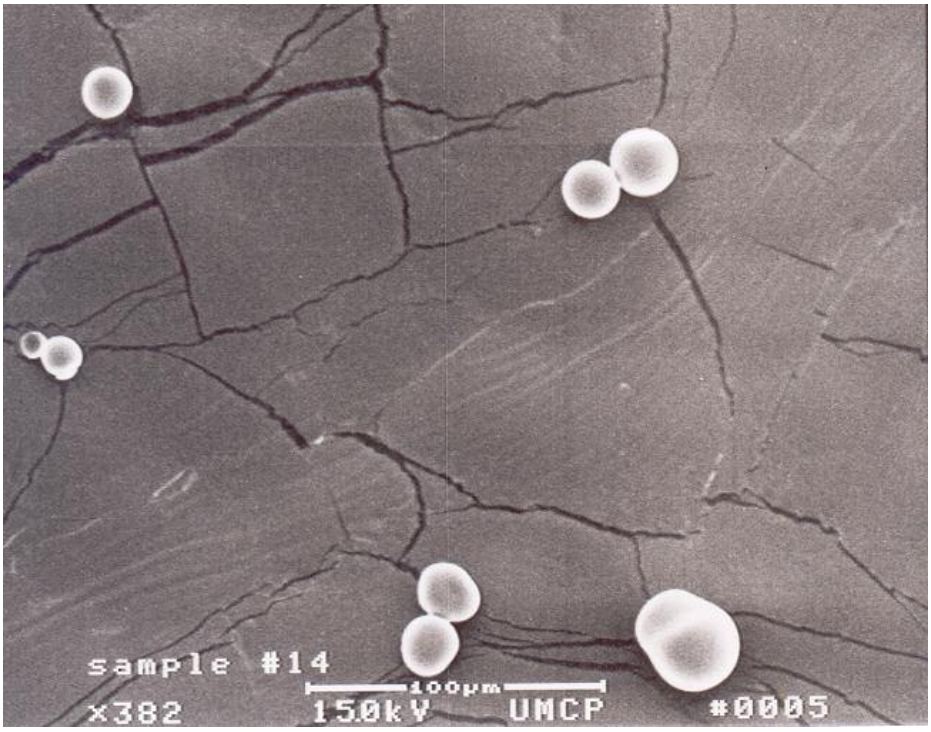

The result of sample 15, taken at the experimental point of (1, 0,-1), is not presented because only two particles were captured. The particles were small, essentially spherical, and spaced apart.

5.5. Particle Size Analysis and Frequency Distributions

In most of the above cases, the sample population is large enough that an approximate frequency distribution can be shown for the particle diameter, and size averages can be presented. The number average, surface average, and volume average are calculated from this data. The results for the averages are tabulated in Table 5.4.

Table 5.4. Number Average, Surface Average, and Volume Average for each sample

Sample	Point	Number Average (+/- 5μm)	Surface Average (+/- 5μm)	Volume Average (+/- 5μm)
1	(0,0,0)	18.5	19.2	19.8
2	(0,1,-1)	17.0	17.5	18.0
3	(0,-1,1)	28.1	30.3	32.5
4	(-1,0,-1)	21.3	21.7	22.1
5	(1,-1,0)	55.0	55.1	55.1
6	(-1,0,1)	4.0	4.2	4.4
7	(0,0,0)	25.8	27.0	28.3
8	(-1,-1,0)	30.5	34.0	36.6
9	(-1,1,0)	26.7	30.4	33.4
10	(1,1,0)	13.1	13.4	13.6
11	(0,0,0)	23.5	23.8	24.1
12	(0,-1,-1)	17.5	18.0	18.5
13	(1,0,1)	35.0	39.4	43.2
14	(0,1,1)	18.9	19.4	19.9
15	(1,0,-1)	20.0	20.6	21.2
16	(0,0,0)	15.1	15.9	16.6
17	(0,0,0)	21.2	24.1	26.2

A frequency distribution of the samples in which a particular factor was held constant is presented next. In some instances, the distributions were not helpful because of missing samples or small population size resulting in a misleading spread. Figure 5.13 shows the samples in which the concentration is held at its lowest value. This figure is followed by runs at the middle and high concentration values (Figures 5.14 and 5.15). For all the subsequent distributions, the trendlines are only shown as visual guides and are not statistical fits to the data.

Figure 5.13. Frequency Distribution for C = 2.88 M

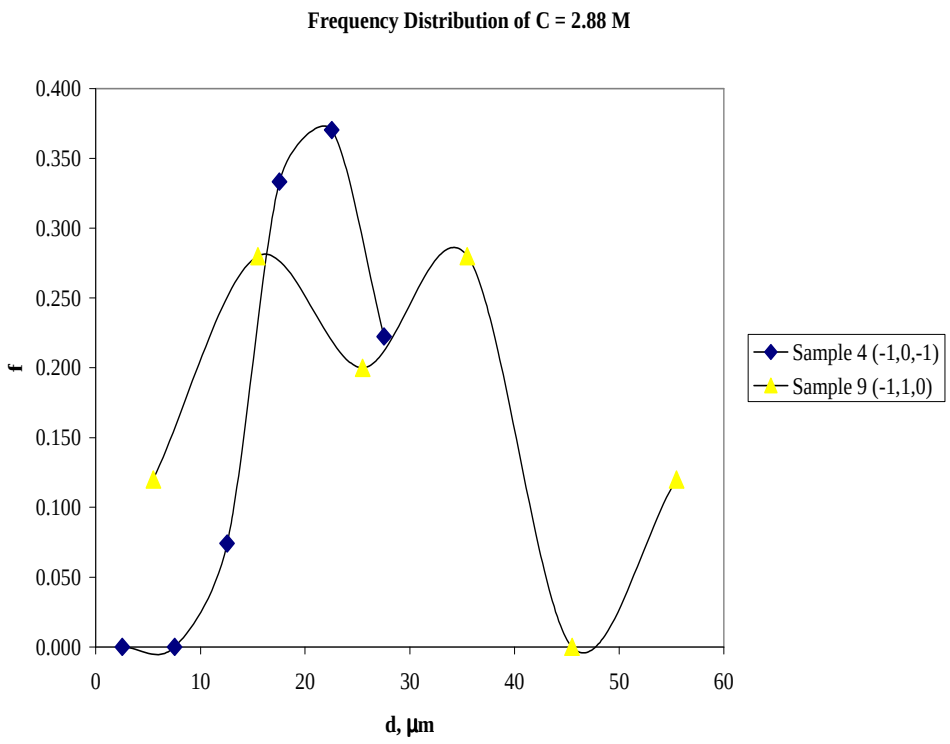

Figure 5.13 shows a bimodal distribution for sample 9. The general trend is that diameter increases with increasing flow rate and temperature for C = 2.88 M. This distribution cannot confirm this because some other combination of samples (i.e. sample 8) are missing.

Figure 5.14. Frequency Distribution for C = 3.52 M

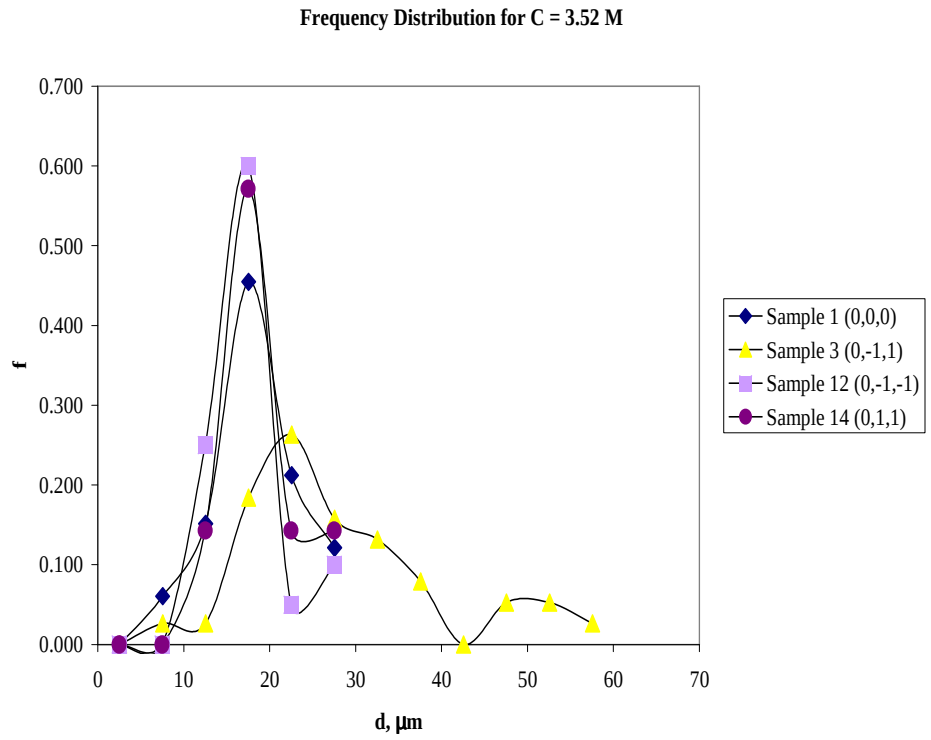

Most of the distributions have a mean near 20 µm. The only trends that can be visually elucidated are that particle size decreases as flow rate (samples 3 and 14) and temperature (samples 3 and 12) increase.

Figure 5.15. Frequency Distribution for C = 4.16 M

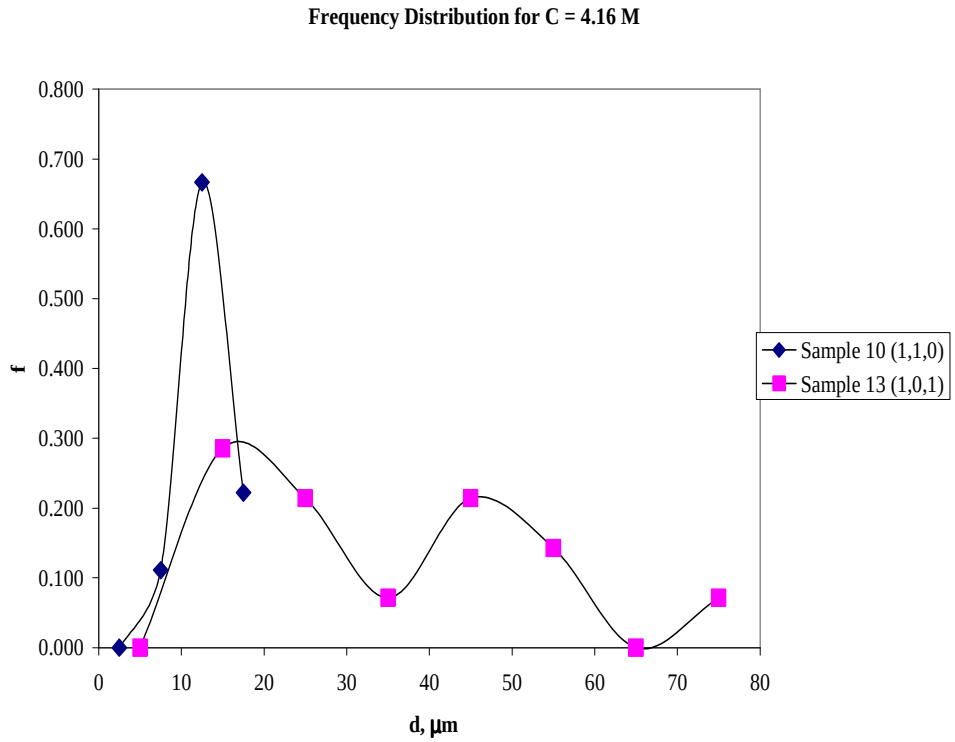

Sample 13 also has a bimodal distribution. This figure suggests that particle size increases as flow rate decreases from 1 to 0.

The following distributions (Figures 5.16-18) show the distributions over the changing levels of flow rate.

Figure 5.16. Frequency Distribution for Q = 15 mL/min

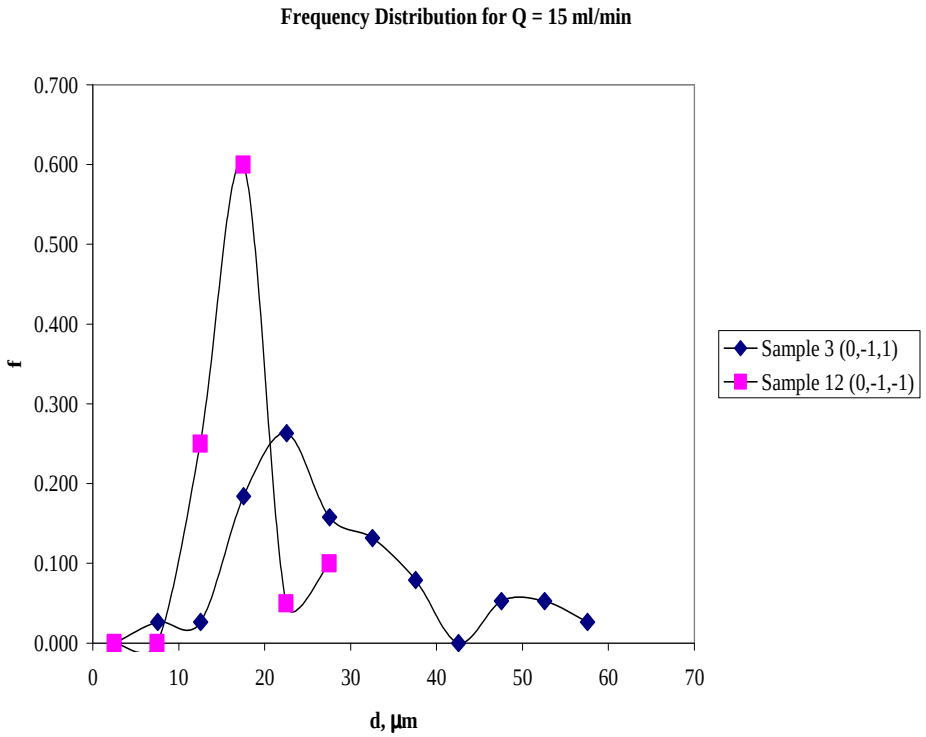

It appears from Figure 5.16 that as temperature increases, particle diameter increases.

Figure 5.17. Frequency Distribution for Q = 20 mL/min

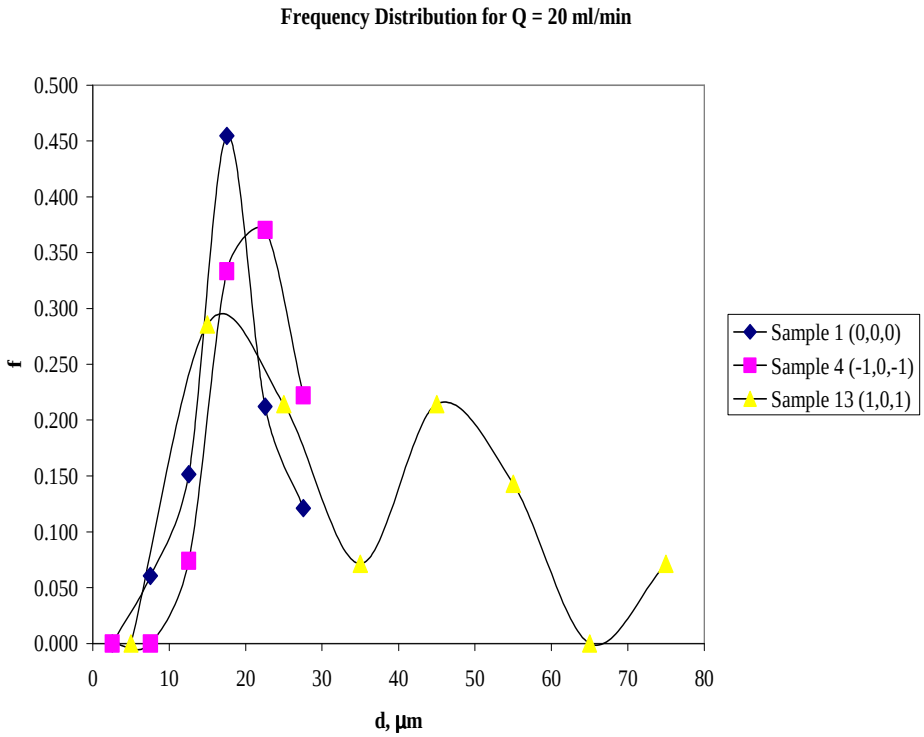

It is difficult to recognize a trend in Figure 5.18 because of the missing design point (samples 6 and 15) and the variance in the center points (sample 1 was chosen to represent the center points).

Figure 5.18. Frequency Distribution for Q = 25 mL/min

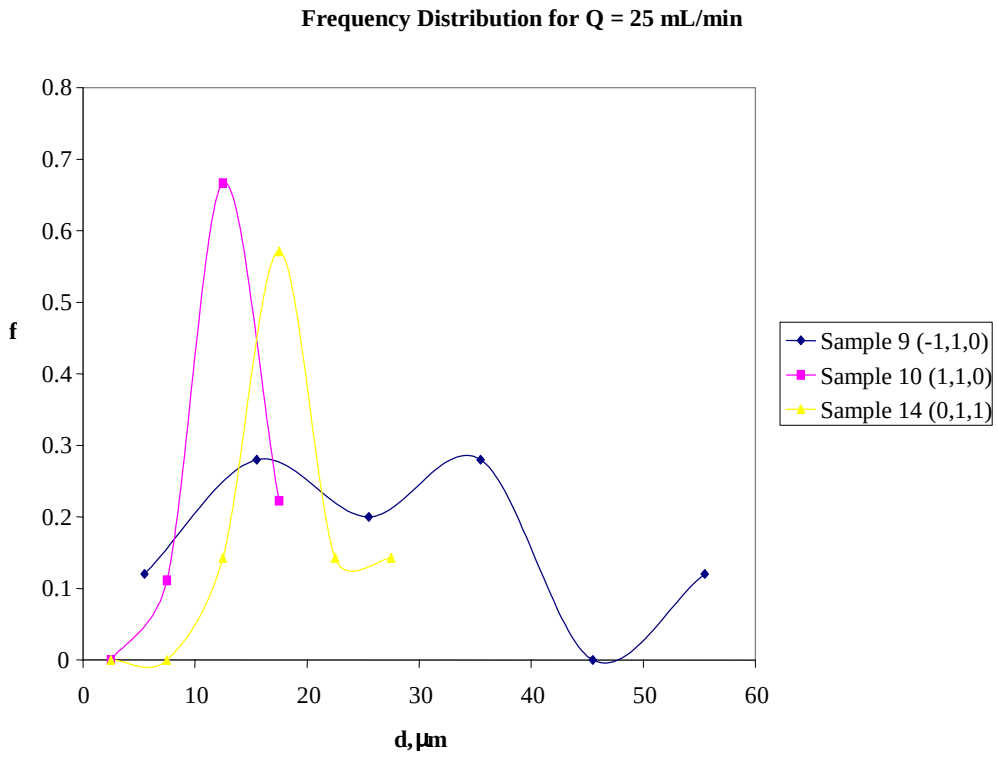

No definitive trend can be observed in Figure 5.18.

The last set of distributions show the effect of va rying temperature. Figures 5.19-21 are the frequency distributions for temperature from its low to its high value.

Figure 5.19. Frequency Distribution for T = 50 ^{0}C

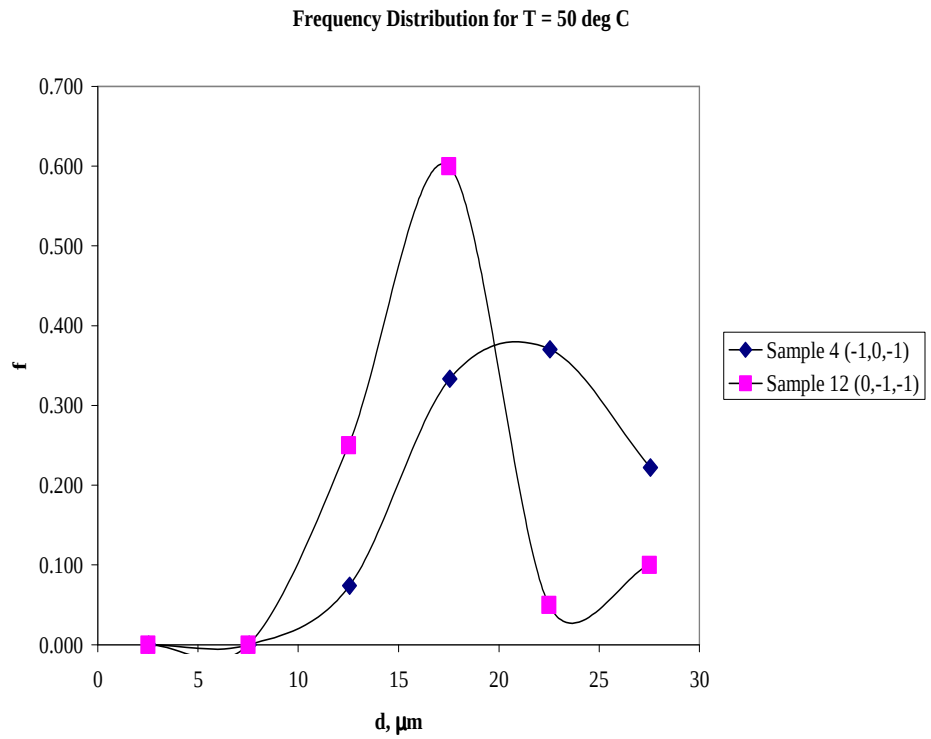

It appears that the particle diameter increases as concentration increases and flow rate decreases for T = 50 ^{0}C.

Figure 5.20. Frequency Distribution for T = 75 ^{0}C

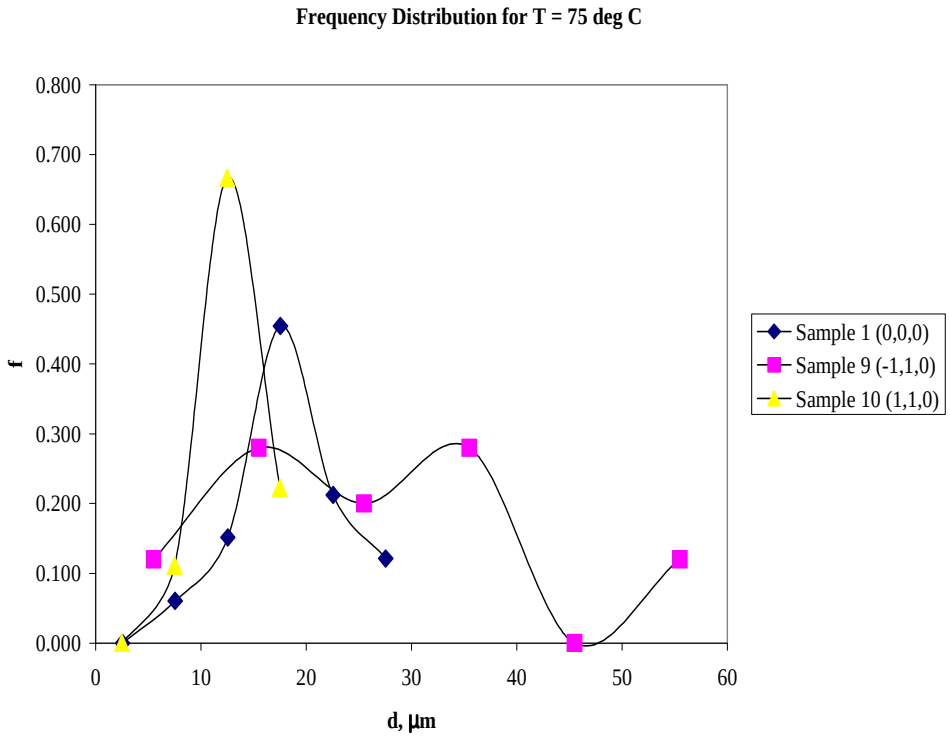

No assumption can be made on a trend from the figure above.

Figure 5.21. Frequency Distribution for T = 100 ^{0}C

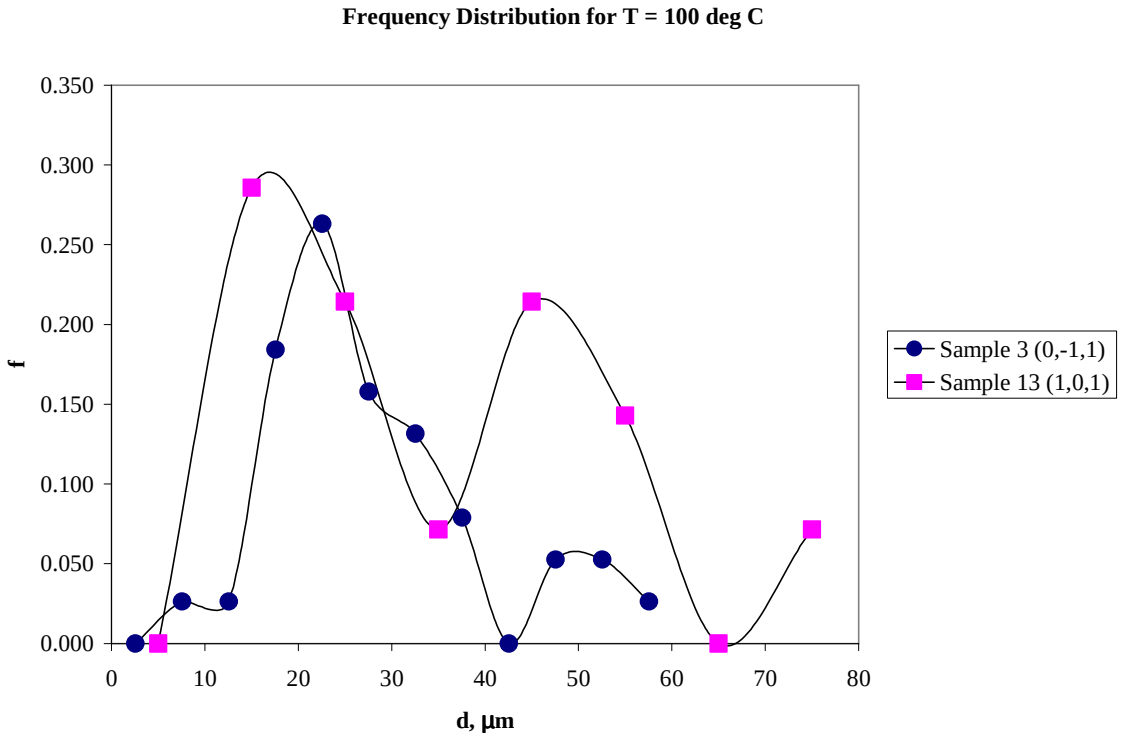

Figure 5.21 above shows that particle size increases with both increasing concentration and increasingflow rate.

5.6. The Results for BET Specific Surface Area Analysis

In performing the surface area analysis with the NOVA 1200 gas analyzer, each sample was first out-gassed for 2 hours at 110 ^{0}C, and then the specific surface area (A_{sp}) of the primary particles was analyzed by the 6-point BET method using nitrogen gas as the adsorbate. The computer-generated results for this multi-point BET are shown in Table 5.5.

Table 5.5. Specific Surface Area (A_{sp}) for Silica Particle Samples

Sample	Design Point	A_{sp} (m^2/g)
1	(0,0,0)	342.5
2	(0,1,-1)	287.5
3	(0,-1,1)	145.4
4	(-1,0,-1)	200.9
5	(1,-1,0)	258
6	(-1,0,1)	156.2
7	(0,0,0)	123
8	(-1,-1,0)	172
9	(-1,1,0)	146.3
10	(1,1,0)	315
11	(0,0,0)	250.8
12	(0,-1,-1)	288.3
13	(1,0,1)	19.9
14	(0,1,1)	100.6
15	(1,0,-1)	210.5
16	(0,0,0)	156.6
17	(0,0,0)	108.5

The results will be statistically treated. Comparisons will be made across factors and between responses. The mathematical models will be derived in chapter six.

6. DISCUSSION

As promised, the results will be more rigorously analyzed and compared in this chapter. An extensive utilization of the software package, Design-Expert, is carried out on the results from the acoustodispersion precipitation experiments. This package is useful because it is integrated with the Box-Behnken experimental design and therefore selects the appropriate statistical tools to test the validity of both the results and the design itself. This chapter presents the analysis of the different diameter averages from the previous chapter by looking at the analysis of variance, or ANOVA, and employing linear regression analysis, when suitable. The mathematical model from the regression analysis will be presented, using the number average diameter. ANOVA will also be performed on the specific surface area results and linear regression will be used to derive the mathematical model that can be used to predict surface area from the most significant terms. Discussion will be made regarding the observations made from the SEM images of the particles and the trend of the plots when compared to expected results. Preceding these discussions will be a brief discourse on the main statistical tools employed, such as ANOVA and linear regression.

6.1. Statistical Tools

The analysis of variance (ANOVA) is "…a collection of experimental situations and statistical procedures for the analysis of quantitative responses from experimental units" (Devore 2000). ANOVA involves the result from the F-Test, which is used for testing the null hypothesis that the means are identical. The null hypothesis is rejected when the f value (calculated using ANOVA) is greater than the F value (obtained from an F table), at a certain significance (throughout this analysis, a significance of $\alpha = 0.1$ will be applied). ANOVA can also measure the interaction among factors and their significance to the model. Finally, a normal probability plot can be used to graphically determine if the mean response corresponds to a normal distribution. If the residuals fit a linear curve, then the variation of the random error term (denoted by $E(\varepsilon)$ in Equation 4.2) is negligible.

This analysis will be combined with regression analysis in deriving the mathematical model. Regression analysis is simply the investigation of the relationship between variables (Devore 2000). The correlation coefficient, r, is a unitless (derived from the standard deviation) quantitative measure of the extent to which the variables are related. The software utilized throughout the paper is very user-friendly in performing statistical analysis.

Once a model is suggested, its aptness should be verified. Model adequacy can be tested by calculating the residuals, which is the predicted

response minus the actual response, and plotting it against the various function. The models in question in this project are checked by the normal probability plot, and the Studentized (normalized) residuals versus the factors. The latter plot is the one most recommended for multiple regression analysis (Devore 2000) and should show random scatter within the standard deviation range. In this chapter, the factor terms of concentration (C), flow rate (Q), and temperature (T), are referred to by the Design-Expert software as A, B, and C, respectively.

6.2. Analysis of Number Average Diameter

The figures below represent the response of number average diameter (a measured value) to each of the three factors (coded values). Figure 6.1 is for the concentration factor. This graph indicates that there is a weak relationship of concentration versus number average diameter, an observation which the correlation coefficient ($r = 0.328$) supports. One possibility for the weak relationship is that the factor is significant within an interaction term. It is expected that the particle size would increase with sodium silicate concentration due the larger number of primary particles available for aggregation. In addition, shrinkage would play a weaker role when more primary particles are present within the gel particle.

Figure 6.1. Number Average Diameter vs. Concentration

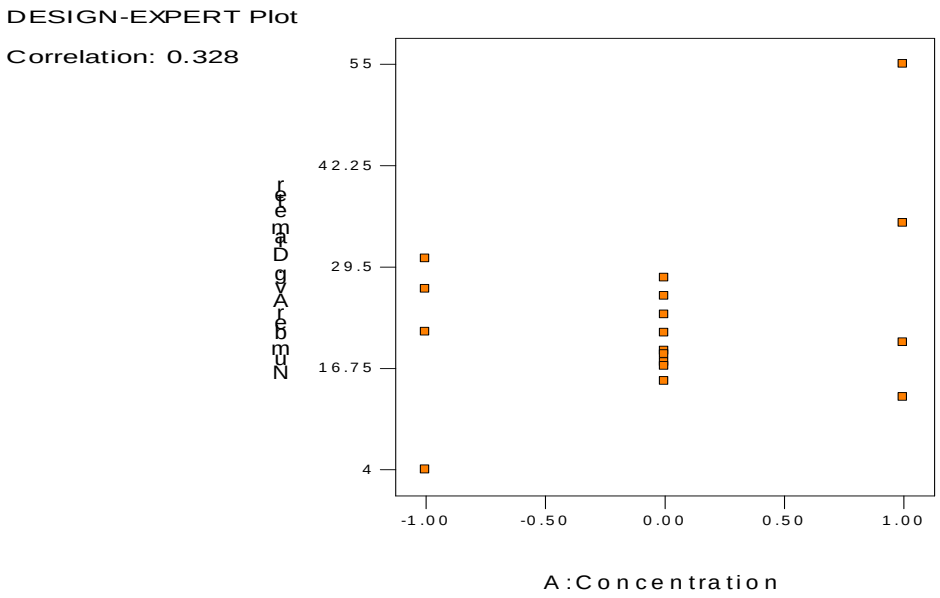

Figure 6.2 is the effect of the flow rate factor on number average diameter. This figure seems to indicate that the diameter decreases as flow rate increases with a fairly moderate correlation (r = -0.448). No literature has been found that gives the effect of flow rate on droplet size for ultrasonic atomization at a constant frequency, but Berger (2001) reports droplet sizes of 4 – 68 μm for a frequency of 100 kHz. Intuition would suggest that the particle size would decrease with increasing flow rate since the liquid is being forced more rapidly through the orifice and is more able to overcome the liquid/air interfacial tension. Conversely, one could also

expect more coalescence of droplets at the nozzle exit due to the increase in number concentration of droplets.

.

Figure 6.2. Number Average Diameter vs. Flow Rate

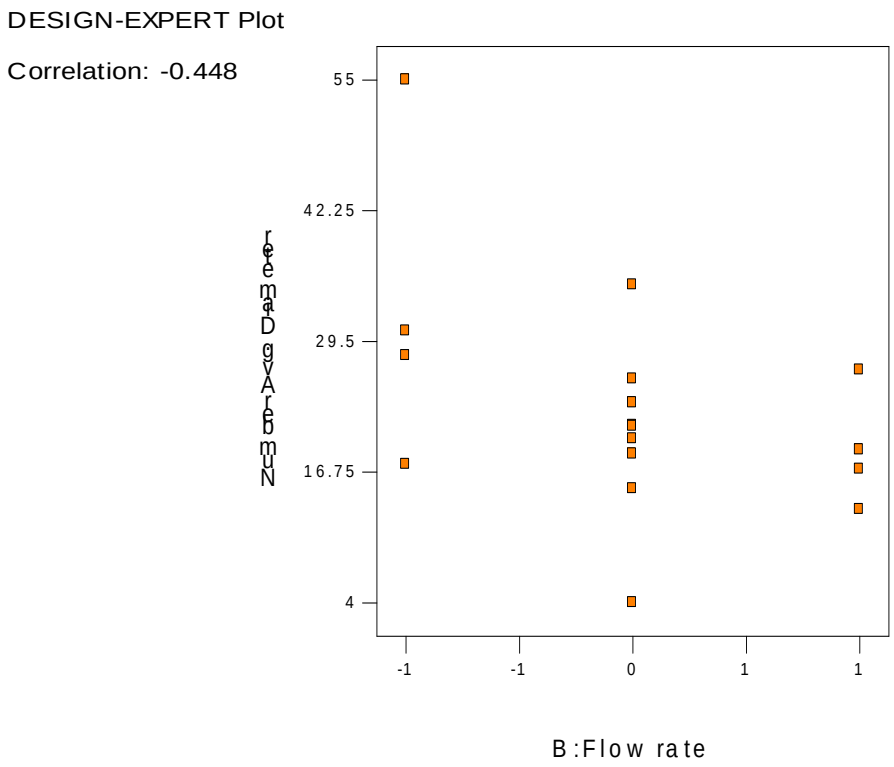

Figure 6.3 corresponds to the temperature factor

Figure 6.3. Number Average Diameter vs. Temperature

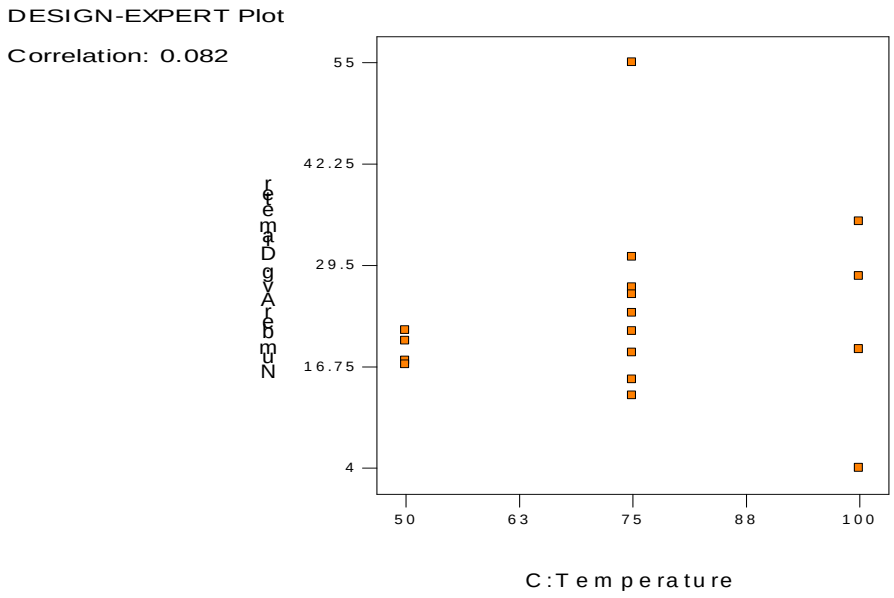

The data suggests relationship between temperature and number average diameter is the least discernable of the three factors. The correlation value of 0.082 nears zero. Intuition would expect that particle size would decrease with increasing temperature because the water in the particles is being evaporated at a faster rate. The ANOVA table for the quadratic model (Table 6.1) is printed below to show the significant terms.

The F-test values indicate that the quadratic model is significant because the terms fall way below the significance value of 0.1. The other significant values are A (concentration), B (flow rate), and the interaction between AB and AC. In fact, the interaction graphs show that there is

significant interaction between concentration and temperature at the middle value of flow rate (Figure 6.4), but at the low and high values of flow rate (Figure 6.5 a,b), there is very little interaction (signified by the intersecction of the curves).

Table 6.1. ANOVA Table for the Quadratic Model for Number Average Diameter

Source	**Sum of Squares**	**DF**	**Mean Square**	**F Value**	**Prob > F**
Model	1608.11	9	178.68	4.12	0.0377
A	206.05	1	206.05	4.75	0.0657
B	383.64	1	383.64	8.84	0.0207
C	13.01	1	13.01	0.3	0.6011
A^2	109.62	1	109.62	2.53	0.156
B^2	122.89	1	122.89	2.83	0.1363
C^2	143.97	1	143.97	3.32	0.1113
AB	362.9	1	362.9	8.36	0.0233
AC	260.82	1	260.82	6.01	0.044
BC	18.92	1	18.92	0.44	0.5302
Residual	303.79	7	43.4		
Lack of Fit	233.56	3	77.85	4.43	0.0921

Pure			
Error	70.23	4	17.56
Cor			
Total	1911.9	16	

Figure 6.4. Interaction Graph of Concentration and Temperature for the Middle Value of Flow Rate

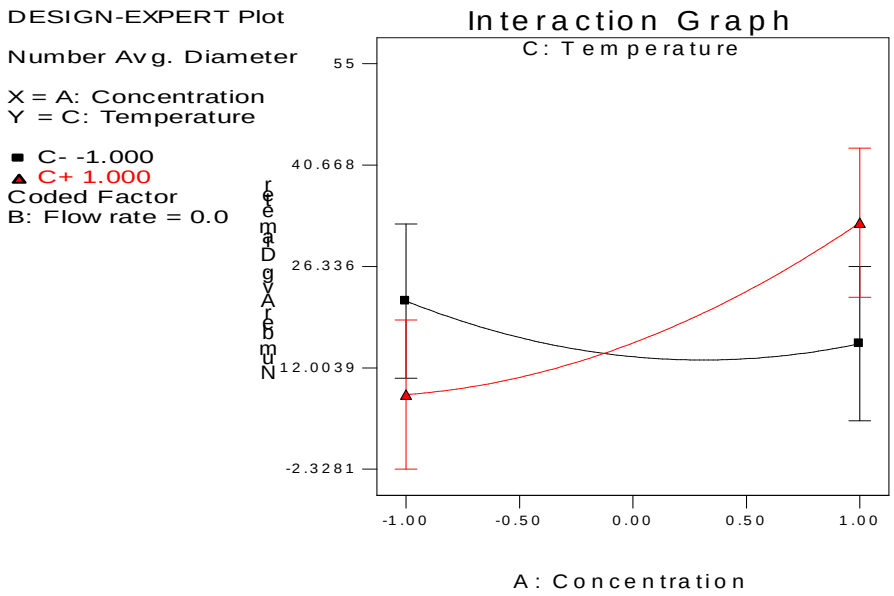

Figure 6.5. Interaction graphs at the (a) low and (b) high value of flow rate

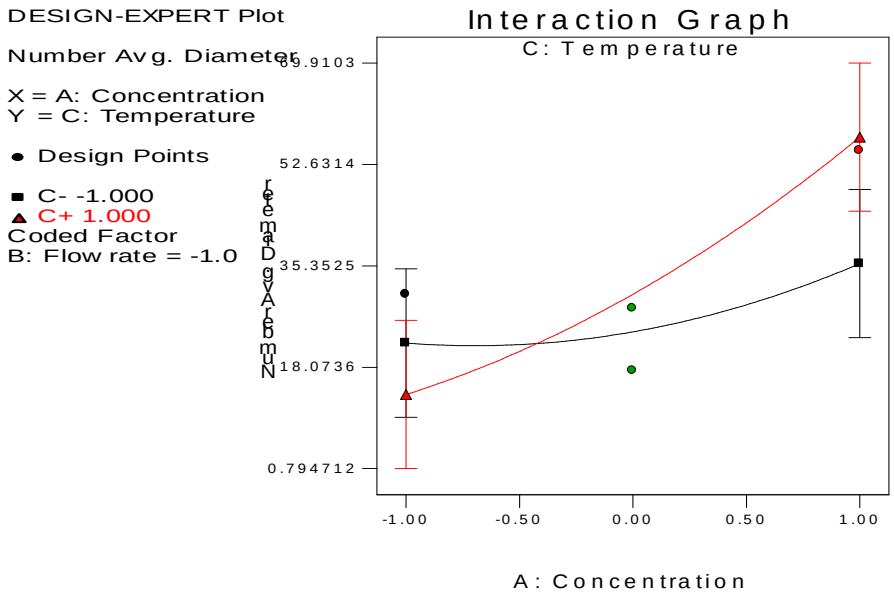

(a)

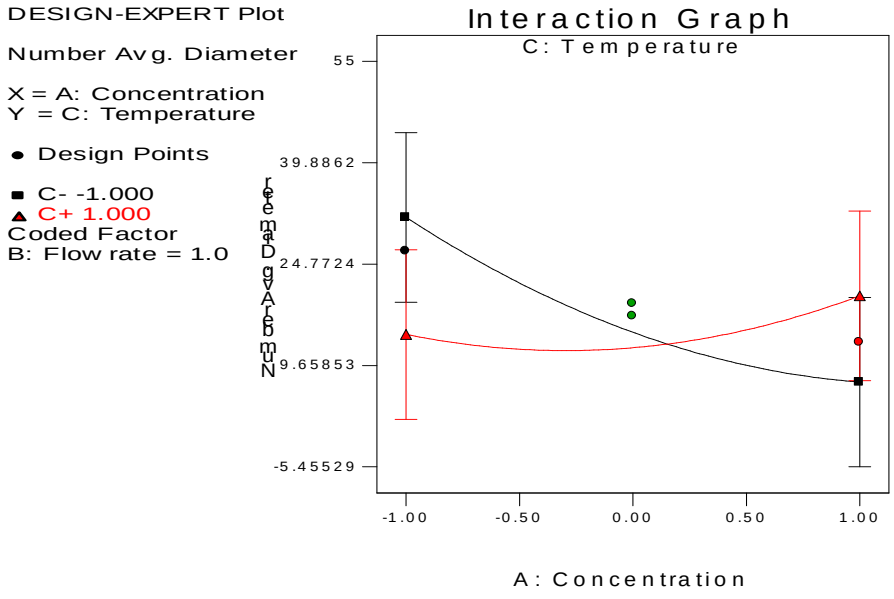

(b)

The final equation derived from this analysis in terms of coded factors is presented below and it includes the slightly insignificant temperature term:

$$\mathbf{d_{NA}} = (5.08 +/- 2.33)\ A + (-6.92 +/- 2.33)\ B + (-9.53 +/- 3.29)\ A*B + (8.08 +/- 3.29)A*C + (20.8 +/- 2.95) \quad (6.1)$$

$\sigma = 6.59$

$r^2 = 0.841$,

where d is diameter, σ is the standard deviation, and r^2 is the square of the correlation. Concentration and flow rate interact to decrease the particle diameter. Although there are more primary particles at higher concentrations of sodium silicate, the overcoming force provided by higher flow rates on surface tension may win out in certain regions of temperature. Concentration and temperature interact to increase the particle diameter. Temperature may have more of an effect when the apparent density (or the packing of the primary particles) is low, and evaporation of water can more rapidly due to greater pore space.

The diagnostic plots (Figure 6.6 and 6.7) shed further light on the validity of the model.

Figure 6.6. Studentized Normal Probability Plot of the residuals for Number Average Diameter

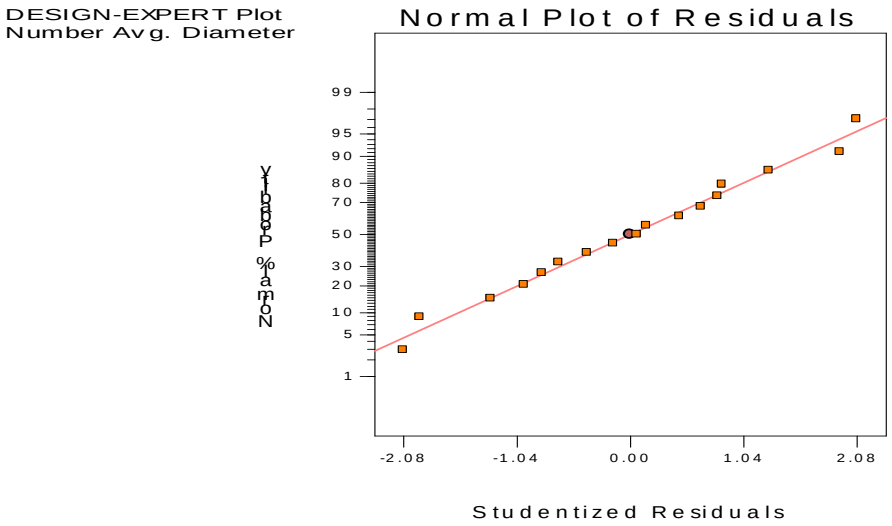

Figure 6.7. Plot of the residuals vs. (a) Concentration (b) Flow Rate and (c) Temperature

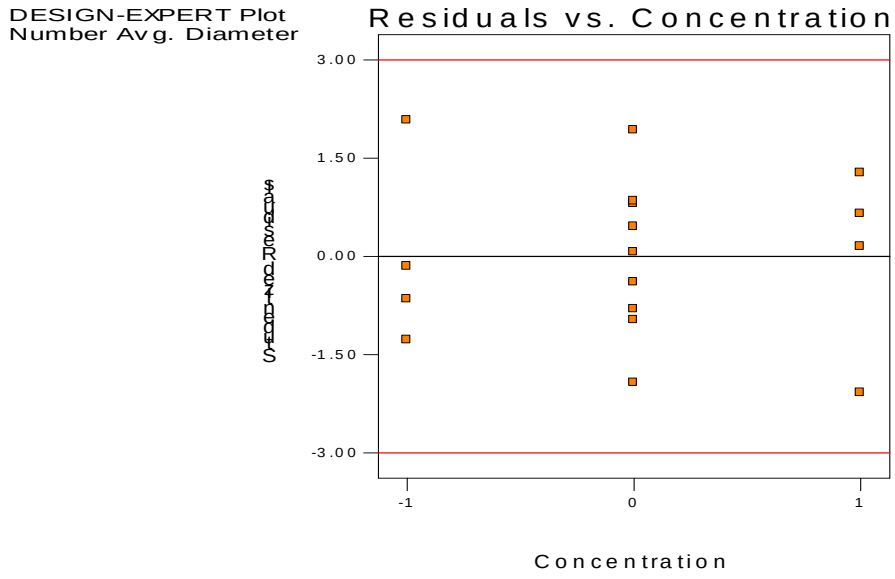

(a)

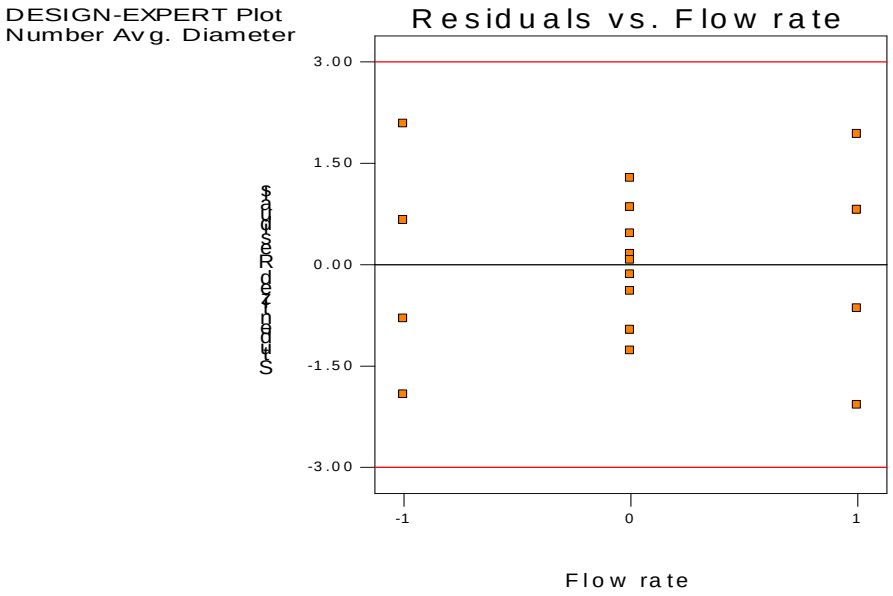
DESIGN-EXPERT Plot
Number Avg. Diameter
Residuals vs. Flow rate
3.00
1.50
0.00
-1.50
-3.00
-1
0
1
Flow rate

(b)

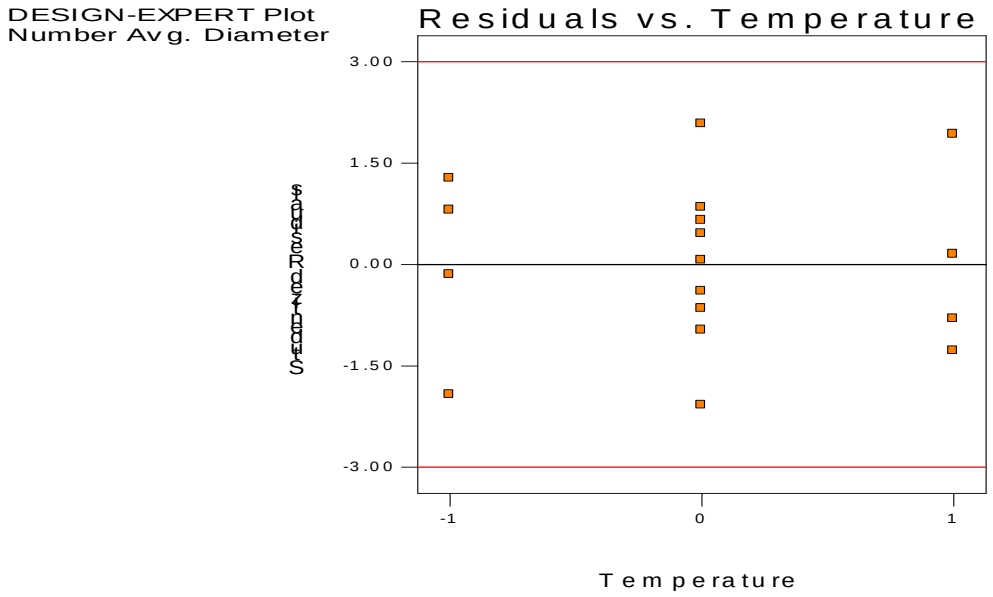
DESIGN-EXPERT Plot
Number Avg. Diameter
Residuals vs. Temperature
3.00
1.50
0.00
-1.50
-3.00
-1
0
1
Temperature

(c)

The normal probability plot is reasonably straight and all of the residual plots versus each factor exhibit random scatter, and all of the points lie within the standard deviation ranges. It can be therefore assumed that the model is a plausible one.

6.3. Analysis of the Surface Average Diameter

The surface average diameter is proportionally larger than the number average diameter because it takes into affect, the surface area of the particle. The correlations don't differ greatly from the number average diameter as shown below:

Concentration: r = 0.295

Flow Rate: r = -0.437

Temperature: r = 0.120

The ANOVA table below (Table 6.2) is an almost exact reflection of the previous model. The BC term is again strongly non-significant (prob >F = 0.4888 for $\alpha = 0.1$).

Table 6.2. ANOVA Table for the Quadratic Model for Surface Average Diameter

Source	Sum of Squares	DF	Mean Square	F Value	Prob > F
Model	1746.61	9	194.068	3.83044	0.0452
A	*182.405*	*1*	*182.405*	*3.60024*	*0.0996*
B	*401.861*	*1*	*401.861*	*7.93179*	*0.0259*
C	*30.0313*	*1*	*30.0313*	*0.59275*	*0.4665*
A^2	*136.8*	*1*	*136.8*	*2.70011*	*0.1443*
B^2	*128.529*	*1*	*128.529*	*2.53686*	*0.1552*
C^2	*163.161*	*1*	*163.161*	*3.2204*	*0.1158*
AB	*362.903*	*1*	*362.903*	*7.16284*	*0.0317*
AC	*329.423*	*1*	*329.423*	*6.50202*	*0.0381*
BC	*27.04*	*1*	*27.04*	*0.53371*	*0.4888*
Residual	354.653	7	50.6646		
Lack of Fit	*276.953*	*3*	*92.3175*	*4.75251*	*0.0831*
Pure Error	*77.7*	*4*	*19.425*		
Cor Total	2101.26	16			

The major difference is that the temperature term is much more strongly non-significant. The equation below is the response related with the significant terms (in coded factors).

$$\mathbf{d_{SA}} = (4.77 +/- 2.52)\ A + (-7.09 +/- 2.52)\ B + (-9.52 +/- 3.56)\ A*B + (9.08 +/- 3.52)\ A*C + (22.0 +/- 3.18) \quad (6.2)$$

$\sigma = 7.12$

$r^2 = 0.831$

The normal probability plot (Figure 6.8) and the residual plots (Figure 6.9) suggest that the quadratic model is appropriate, though the standard deviation above is slightly larger than that for the number average diameter.

Figure 6.8. Studentized Normal Probability Plot of the residuals for Surface Average Diameter

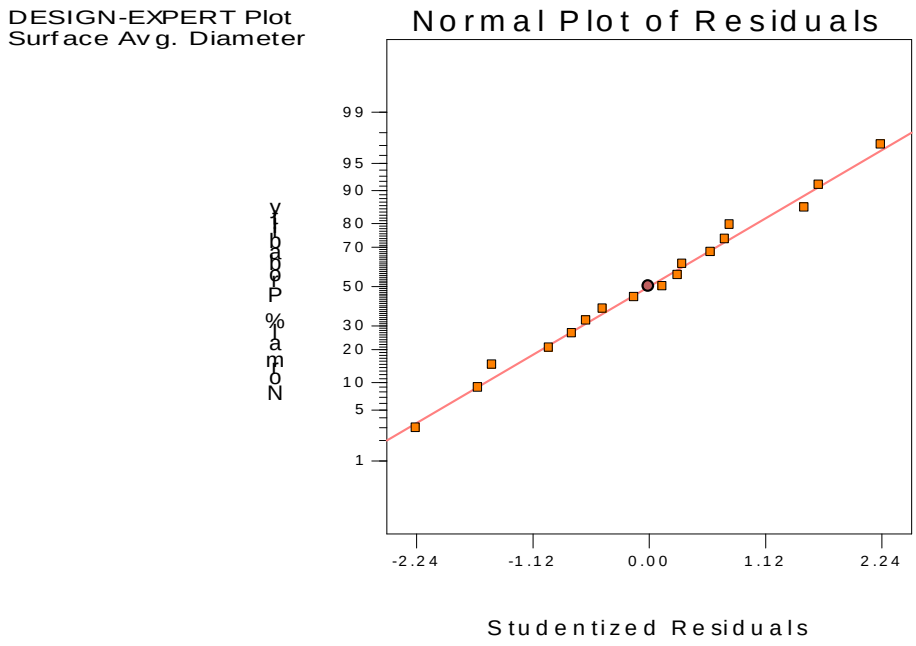

Figure 6.9. Plot of the residuals vs. (a) Concentration (b) Flow Rate and (c) Temperature

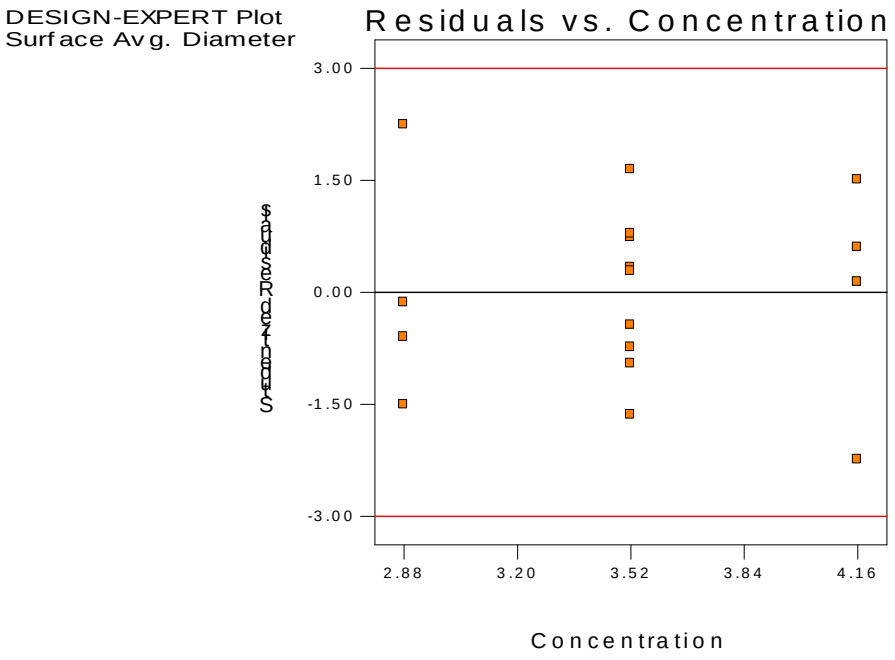

(a)

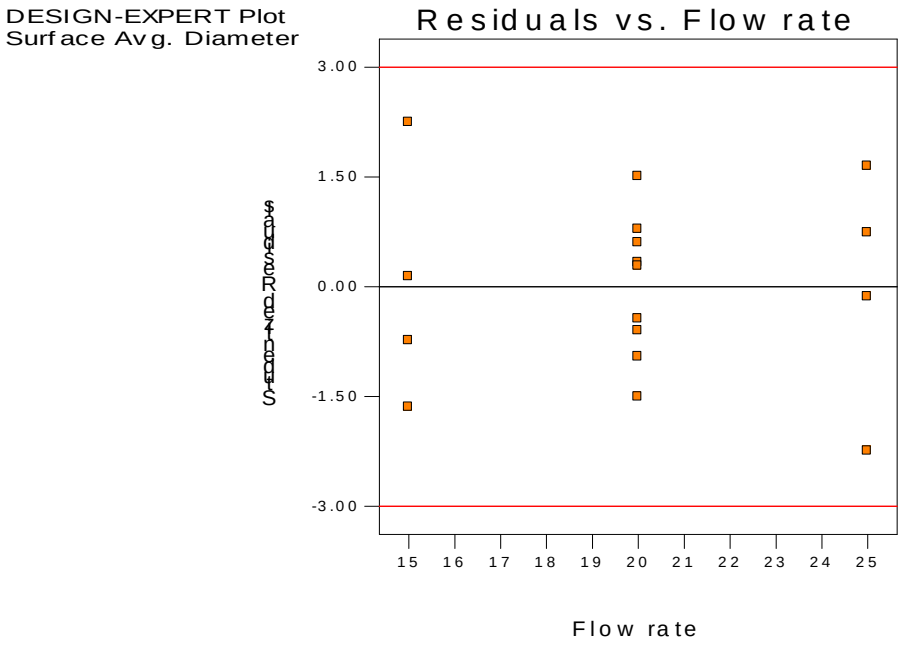
DESIGN-EXPERT Plot
Surface Avg. Diameter
Residuals vs. Flow rate
3.00
1.50
0.00
-1.50
-3.00
15 16 17 18 19 20 21 22 23 24 25
Flow rate

(b)

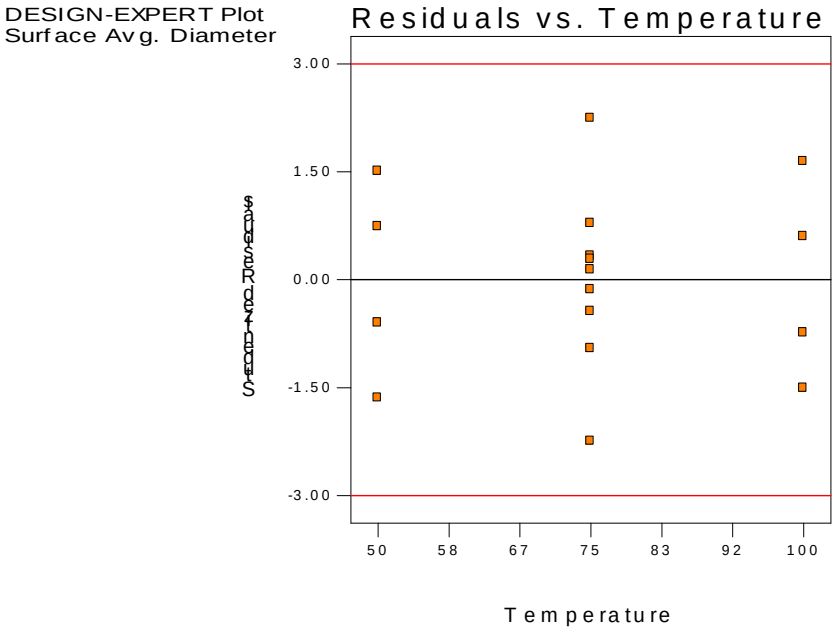
DESIGN-EXPERT Plot
Surface Avg. Diameter
Residuals vs. Temperature
3.00
1.50
0.00
-1.50
-3.00
50 58 67 75 83 92 100
Temperature

(c)

6.4. Analysis of the Volume Average Diameter

The volume average is the largest of the averages. The ANOVA table (Table 6.3) indicates here that concentration is weakly insignificant.

Table 6.3. ANOVA Table for the Quadratic Model for Volume Average Diameter

Source	**Sum of Squares**	**DF**	**Mean Square**	**F Value**	**Prob > F**
Model	1875.08	9	208.342	3.43588	0.0589
A	*167.445*	*1*	*167.445*	*2.76143*	*0.1405*
B	*417.605*	*1*	*417.605*	*6.88695*	*0.0342*
C	*51.005*	*1*	*51.005*	*0.84115*	*0.3896*
A2	*156.032*	*1*	*156.032*	*2.57321*	*0.1527*
B2	*131.453*	*1*	*131.453*	*2.16787*	*0.1844*
C2	*170.448*	*1*	*170.448*	*2.81095*	*0.1375*
AB	*366.723*	*1*	*366.723*	*6.04782*	*0.0435*
AC	*394.023*	*1*	*394.023*	*6.49804*	*0.0382*
BC	*36.6025*	*1*	*36.6025*	*0.60363*	*0.4626*
Residual	424.46	7	60.6371		
Lack of Fit	*333.72*	*3*	*111.24*	*4.90368*	*0.0793*
Pure Error	*90.74*	*4*	*22.685*		
Cor Total	2299.54	16			

The equation below is a model of the significant terms

$\mathbf{d_{VA}}$ = (-7.22 +/- 2.75) B + (– 9.58 +/- 3.89)A*B + (9.93 +/- 3.89) A*C + (23.0 +/- 3.48) (6.3)

σ = 7.79

r^2 = 0.815

All of the results for the above analyses indicate that the quadratic model is appropriate, although the poor standard deviation values and poor correlation values show that the lack-of-fit test is significant. The number average diameter shows the best correlation and will be used in subsequent presentation and analysis. To obtain a more reliable model, more replications need to be performed at the face points of the design and better precision needs to be obtained for the center points.

6.5. Specific Surface Area Analysis

Using the statistical techniques and the statistical software employed in the analysis of particle diameter, a mathematical model of the response of specific surface area to the three factors will be presented. The significant terms in the model will be elucidated from the ANOVA table and graphical outputs from regression analysis will be presented in support of the trends suggested by the model.

The graph in Figure 6.10 represents the effect of concentration on surface area.

Figure 6.10. Graph of Specific Surface Area vs. Concentration

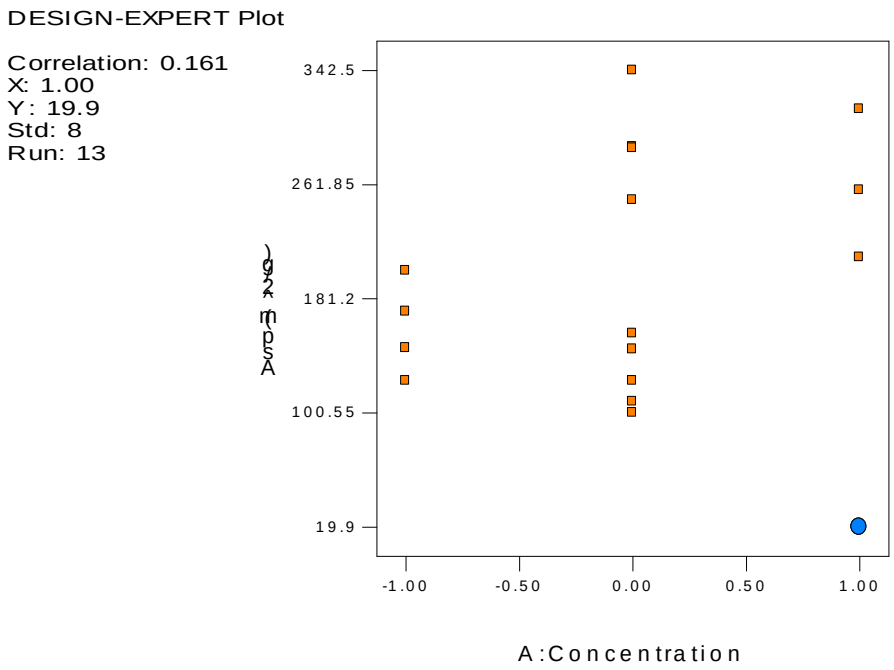

The correlation value of 0.161 indicates that a relationship between specific surface area and concentration is weak. It appears, however, that the highlighted point, Run 13, is a significant contributor to this low correlation value. It has an A_{sp} value of 19.9 m^2/g which differs appreciably from the other samples. This is probably an instrumental error or possible contamination of the sample. From this point, this run will be ignored in the analysis. Figure 6.11 shows the surface area versus concentration graph minus sample 13.

Figure 6.11. Specific Surface Area vs. Concentration (minus sample 13)

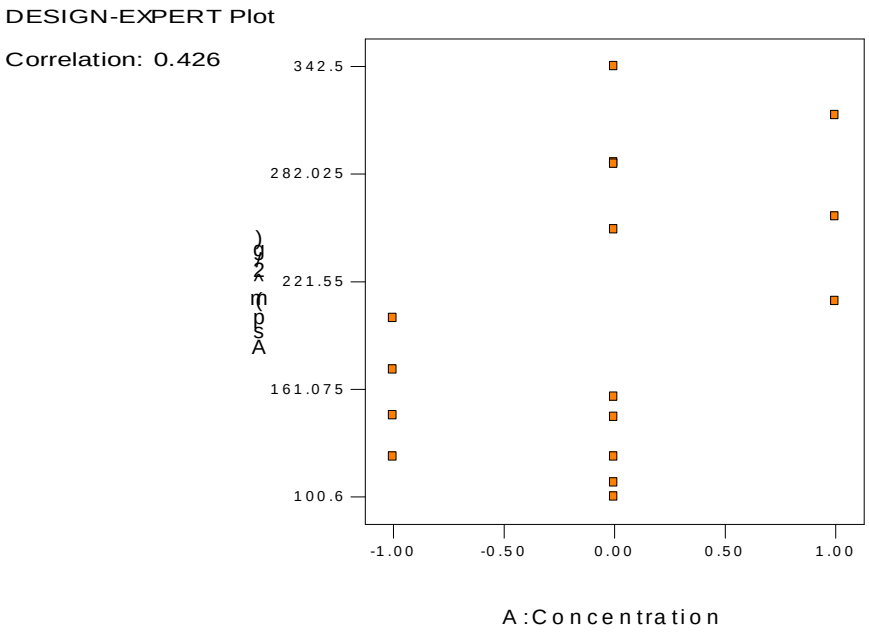

The correlation value jumped to 0.426, which suggests that there is a better correlation without the anomalous point. For a particle of constant density, an increase in primary particles would result in an increase in surface area per gram, as the data suggests. Figure 6.12 shows the plot of surface area versus flow rate.

Figure 6.12. Graph of Specific Surface Area vs. Flow Rate

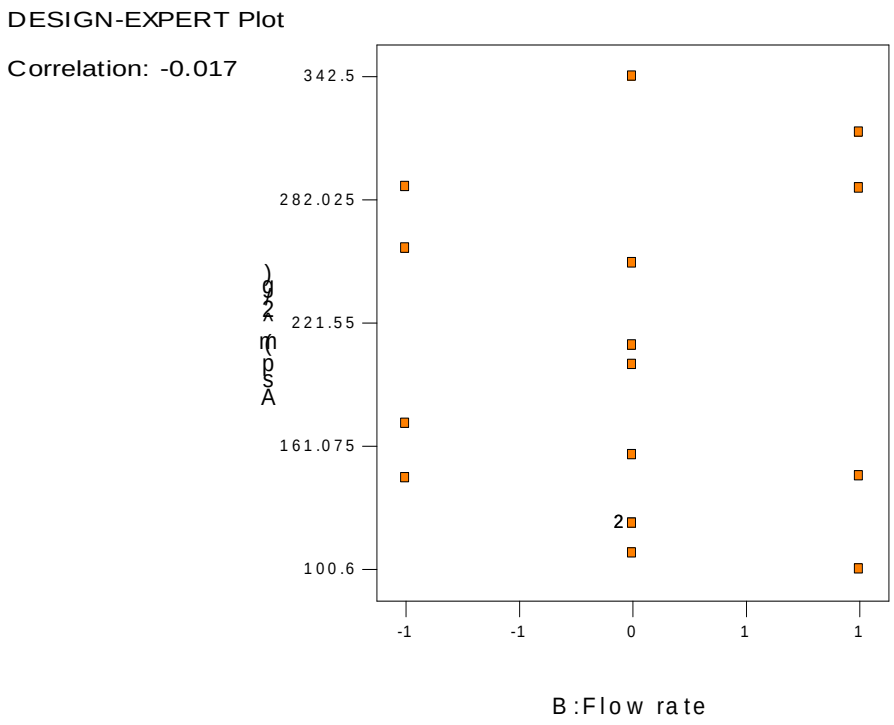

This graph clearly exhibits no definitive trend. The weak correlation value of r = -0.017 only suggests that any contribution of flow rate to surface area is negative. Figure 6.13 showsthe relationship between surface area and temperature.

Figure 6.13. Graph of Specific Surface Area vs. Temperature

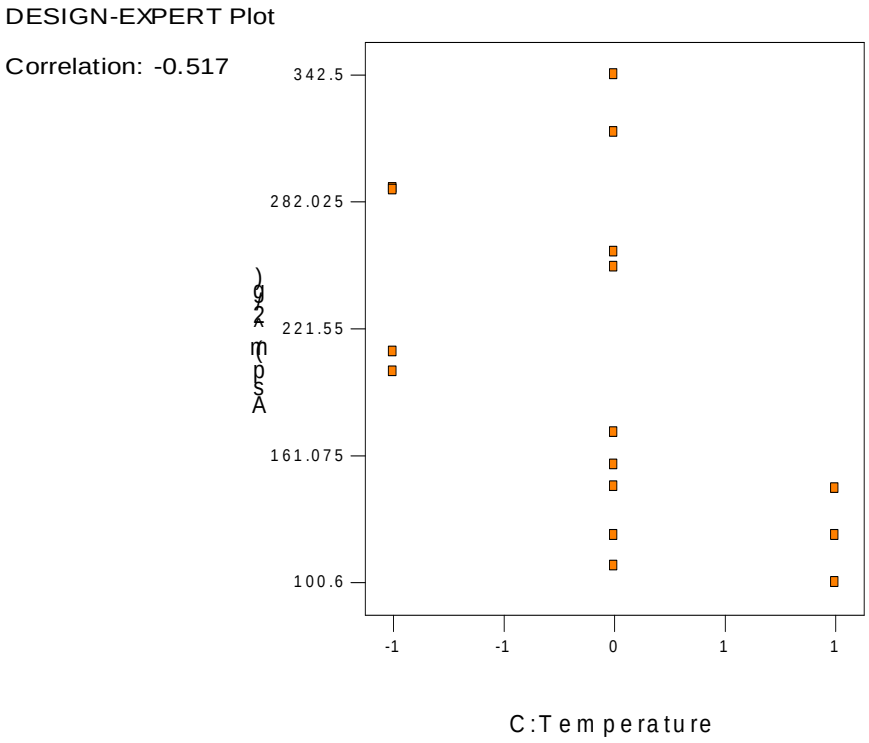

This plot shows that there is a moderate inverse relationship between specific surface area and temperature. It is the strongest relationship of the three factors, with r = -0.517. This may be explained by the collapse of micro and meso pores due to densification (Li, et al 2000) as temperature increases. The ANOVA table (Table 6.4) presented below is the fit summary suggesting which model would be most appropriate based on the sum of squares for a natural logarithm transform of the data.

Table 6.4. Fit Summary of Different Models

Source	Sum of Squares	DF	Mean Square	F Value	Prob > F
Mean	438.1966	1	438.1966		
Linear	1.046544	3	0.348848	3.06337	0.0692
2FI	0.090081	3	0.030027	0.211716	0.8858
Quadratic	0.101719	3	0.033906	0.17318	0.9107
Cubic	0.230746	2	0.115373	0.488878	0.6457
Residual	0.94398	4	0.235995		
Total	440.6097	16	27.53811		

The linear model probability is below the significance threshold of 0.1. It is therefore suggested as the best model to fit to the data. Table 6.5 shows the ANOVA results and the significant terms for the linear model.

Table 6.5. ANOVA Table of the Linear Model for Specific Surface Area

Source	Sum of Squares	DF	Mean Square	F Value	Prob > F
Model	1.046544	3	0.348848	3.06337	0.0692
A	0.24243	1	0.24243	2.128874	0.1702
B	0.013889	1	0.013889	0.121967	0.7330
C	0.644889	1	0.644889	5.663023	0.0348
Residual	1.366526	12	0.113877		
Lack of Fit	0.422546	8	0.052818	0.223811	0.9656
Pure Error	0.94398	4	0.235995		
Cor Total	2.41307	15			

The table shows that concentration is slightly insignificant (prob >F = 0.17 for $\alpha = 0.1$), flow rate is much more strongly insignificant, and

temperature is significant. The mathematical model in terms of the coded factors is presented below of the significant temperature term:

$$\ln \mathbf{A_{sp}} = (-0.57 +/- 0.21)\ C + (5.10 +/- 0.14) \qquad (6.4)$$

$s = 0.59$

$r^2 = 0.376$

The normal probability plot (Figure 6.14) and the Studentized residual plots (Figure 6.15) are shown as added support to the recommended model.

Figure 6.14. Studentized Normal Probability Plot of the Residuals for Specific Surface Area

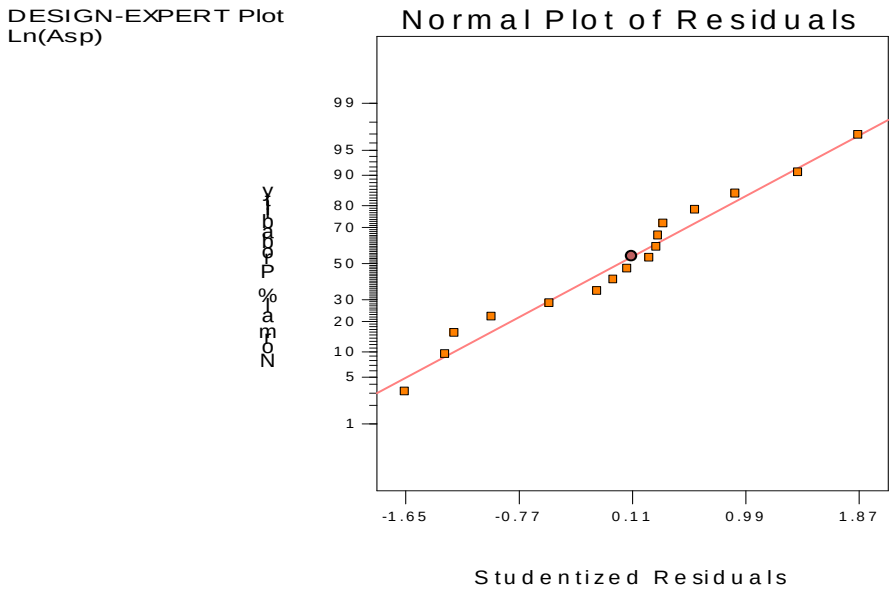

Figure 6.15. Plot of the Residuals vs. (a) Concentration (b) Flow Rate and (c) Temperature

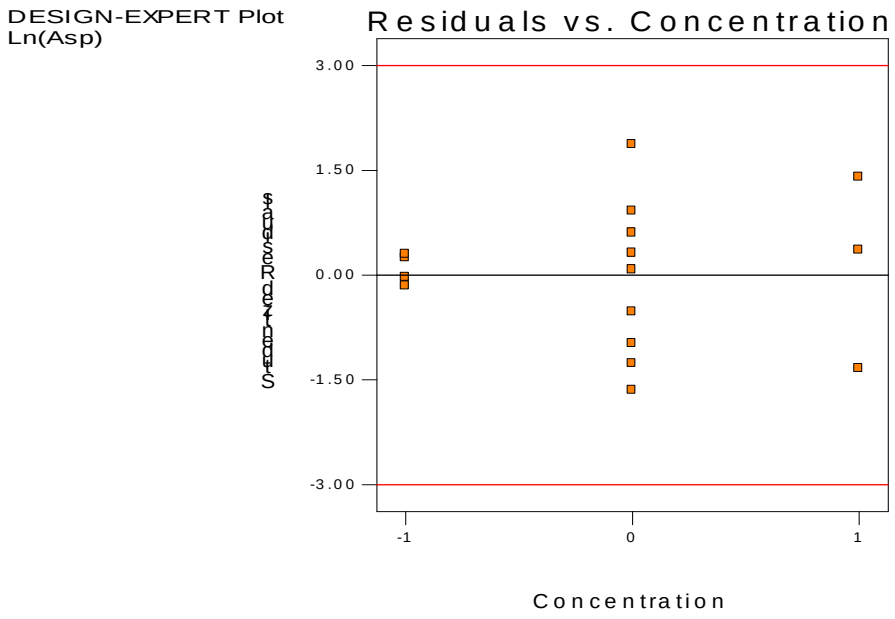

(a)

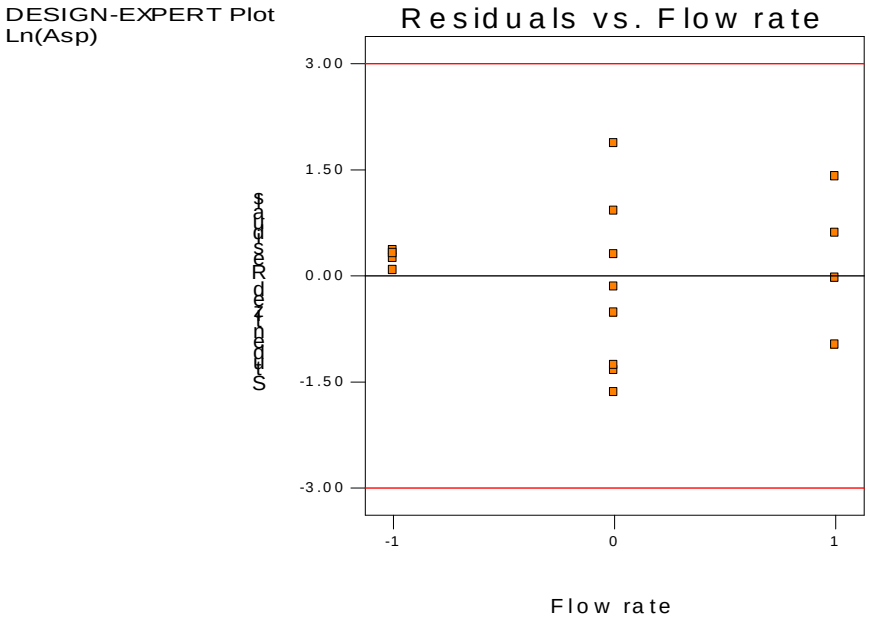
DESIGN-EXPERT Plot
Ln(Asp)
Residuals vs. Flow rate
3.00
1.50
0.00
-1.50
-3.00
Studentized Residuals
-1
0
1
Flow rate

(b)

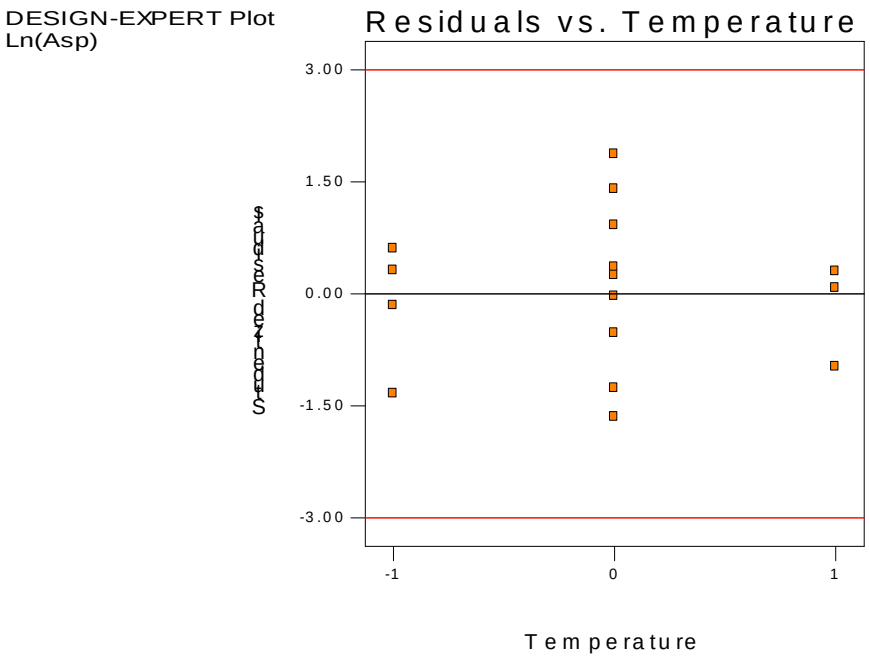
DESIGN-EXPERT Plot
Ln(Asp)
Residuals vs. Temperature
3.00
1.50
0.00
-1.50
-3.00
Studentized Residuals
-1
0
1
Temperature

(c)

The normal probability plot shows a fairly reasonable linear fit and the residual plots all show good random scatter.

7. Conclusion and Further Work

This study of the acoustodispersion precipitation reaction process was a study in reactor design, particle synthesis, and experimental design and analysis. The reactor system itself introduced some novel features to particle synthesis. These features include a continuous flow system that involves low-pressure pumping of only two reactants – sodium silicate and sulfuric acid. The cylindrical mixer induces adequate conditions for turbulent flow and complete mixing. The SEM images confirm that the ultrasonic nozzle is capable of producing spherical silica particles in the size range of 4-55 μm. The heating system required as little as 10 minutes to achieve the required temperature and the system does not necessitate a collecting fluid, as the height of the drying chamber and reaction temperatures were sufficient for complete drying.

This system is fairly quick and inexpensive. As an example, 312 grams of particle can be produced in one hour at a flow rate of 25 mL/min and a sodium silicate concentration of 4.16 M. By contrast, it takes 20 hours to produce micrometer sized silica spheres from 1.79 g of TEOS (Qi, et al., 1998). Problems were encountered in the mixing process when premature gelation sometimes occurred in the mixing cylinder, thus blocking the exit nozzles and backing up the system (the flow rate of the water flush system was not sufficiently high). Possible solutions include using a larger mixer

and wider tubes, and performing continuous gelation experiments to obtain more accurate gelation times.

The examination of the effect of the sodium silicate concentration, volumetric flow rate, and drying temperature on particle diameter and specific surface area has revealed some predictable results and some results that warrant further study. The trend of the response to three factors is undeniably and unsurprisingly complex. A quadratic model, including interaction terms, was suggested from the ANOVA calculations performed by Design-Expert 6.0.4. The result of this model is that number average diameter is proportional to concentration and the interaction of concentration and temperature but inversely proportional to flow rate and the interaction of concentration and flow rate. Temperature is the most insignificant term while flow rate showed the strongest correlation based on a significance of $\alpha = 0.1$. In addition, most of the samples are mono-disperse while a few appear to have a bi-modal distribution.

ANOVA calculations on the data for specific surface area suggested a linear model, a less complicated one. This means that interaction effects are negligible. However, the response is not a linear function of the factors – rather a natural log transformation of the responses was necessary to provide the best linear fit. Once this transformation was performed and the ANOVA calculations were made, the model elucidated stated that the natural log of specific surface area was inversely proportional to temperature and not dependent on flow rate and concentration. The highest

specific surface areas achieved were 315 m^2/g (C = 4.16 M, Q = 25 mL/min, T = 75 ^0C, d_{SA} = 13.4 μm) and 342 m^2/g (C = 3.52 M, Q = 20 mL/min, T = 75 ^0C, d_{SA} = 19.2 μm).

Future work should be done to examine the effect of fluid viscosity and the surface tension of the gelling solution at the air/nozzle interface on particle size and surface area. The temperature generated by the nozzle itself should also be factored in. A study of the porosity of these particles based on the three factors will also be useful information for industrial purposes. Finally, the factor regions should be broadened and more replications should be performed, which may explain erroneous points and produce a more reliable and precise mathematical model of the process.

APPENDIX A: THE BET EQUATION (Hiemenz and Rajagopalan 1997)

A. BET Equation

$$\left(\frac{1}{V}\right)\left(\frac{x}{1-x}\right)=\left(\frac{c-1}{c*V_m}\right)x+\left(\frac{1}{c*V_m}\right)$$

V = volume of gas adsorbed

V_m = volume of gas adsorbed at monolayer coverage

$$x = P/P_0$$

$$c = e^{\left(\frac{e-e_v}{k*T}\right)}$$

B. Linearized BET Equation

$$\left(\frac{1}{V}\right)\left(\frac{x}{1-x}\right)=\left(\frac{c-1}{c*V_m}\right)x+\frac{1}{c*V_m}$$

$$V_m = \frac{1}{m+b}$$

$$c = \frac{m}{b}+1$$

C. Specific Surface Area

$$A_{sp} = S_t / W$$

S_t = total surface area

W = weight (mass) of powder sample

$$S_t = \left(\frac{A}{A_c} \right) V_c \left(\frac{P_a * M_a}{R * T} \right) \left(1 - P / P_o \right)$$

A = sample integrator reading

A_c = calibration integrator reading

V_c = calibration volume

P_a = ambient pressure; P_o is total pressure

T = temperature, R, gas constant

M_a = adsorbate molecular weight

APPENDIX B: DATA FROM THE GELATION TIME EXPERIMENT

Volume fraction of Sodium Silicate (%)	Concentration of sulfuric acid (M)	Gelation Time (s)
45	.45	93
	.50	30
	.55	7
Estimate for gelation time =60 s	**.48**	**60**
55	.50	208
	.52	134
	.54	90
	.56	23
Estimate for gelation time =60 s	**.55**	**60**
65	.45	750
	.50	233
	.55	70
Estimate for gelation time =60 s	**.56**	**60**

APPENDIX C: SEM IMAGES OF OTHER CENTER POINTS

Sample 7

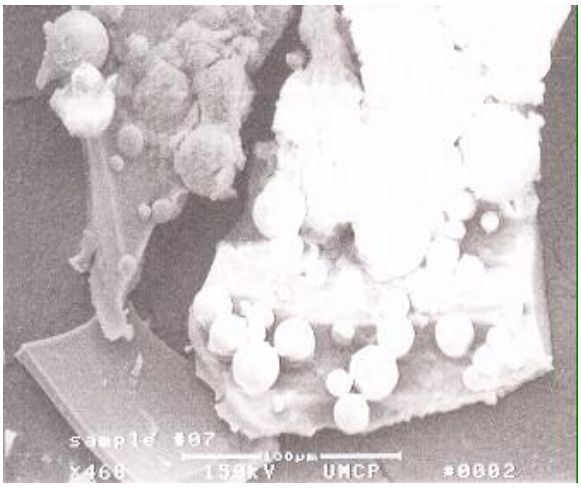

Sample 11

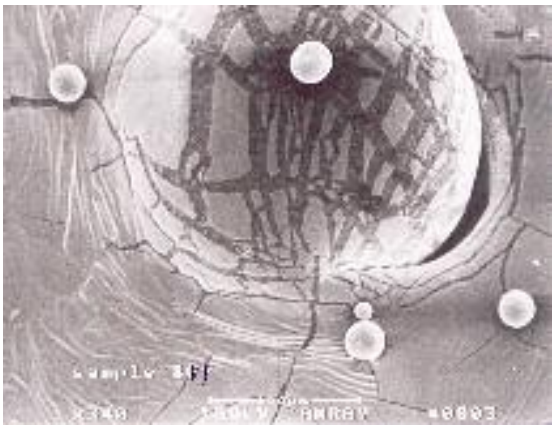

Sample 17

REFERENCES

(1989). Sol-Gel Science and Technology. Winter School on Glasses and Ceramics from Gels, Sao Carlos, Brazil, World Scinetific Publishing.

Amiel, O., J. M. Heintz, et al. (1990). "Preparation of Spherical and Controlled Size Particles of Silica or Tantalum Oxide by Chemical Reaction in Aerosols." Journal of Aerosol Science **21**(6): 799-810.

Anderson, M. and P. Whitcomb (1999). Design-Expert. Minneapolis, MN, Stat-Ease, Inc.

Berger, H. L. (1998). Ultrasonic Liquid Atomization, Theory and Application. Hyde Park, NY, Partridge Hill Publishers.

Devore, J. L. (2000). Probability and Statistics for Engineering and the Sciences. Pacific Grove, CA, Duxbury.

Ganguli, D. and M. Chatterjee (1997). Ceramic Powder Preparation: A handbook. Boston, Kluwer Academic Publishers.

Gerber, T., B. Himmel, et al. (1994). "WAXS and SAXS Investigation of Structure Formation of Gels from Sodium-Waterglass." Journal of Non-Crystalline Solids **175**(2-3): 160-168.

Gerber, T. and B. Knoblich (2001). "Aggregation in SiO2 Sols from Sodium Silicate Solutions." Journal of Non-Crystalline Solids **283**(1-3): 109-113.

Harris, M. T., T. C. Scott, et al. (1993). "The Synthesis of Metal Hydrous Oxide Particles by Multiphase Electrodispersion." Materials Science and Engineering **A168**: 125-9.

Hench, L. L. (1998). Sol-gel silica: processing, properties, and technology transfer. New Jersey, Noyes Publications.

Hiemenz, P. C. and R. Rajagopalan (1997). Principles of Colloid and Surface Chemistry. New York, Marcel Dekker.

Iller, R. K. (1979). The Chemistry of Silica. New York, John Wiley & Sons, Inc.

Kosuge, K. and P. S. Singh (2001). "Rapid Synthesis of Al-Containing Mesoporous Silica Hard Spheres of 30-50 um Diameter." Chemistry of Materials **13**: 2476-2482.

Kraber, S. (2000). Handbook for Experimenters. Minneapolis, MN, Stat-Ease, Inc.

Kresge, C. T., M. E. Leonowicz, et al. (1992). "Ordered Mesoporous Molecular-Sieves Synthesized by a Liquid-Crystal Template Mechanism." Nature **359**(6397): 710-712.

Li, Z.-j., C.-r. Lui, et al. (2000). "Effect of heat treatment on pore structure properties of silica gel powders derived from water glass." Journal of Non-Crystalline Solids **265**: 189-192.

Lide, D. R., Ed. (2000). CRC Handbook of Chemistry and Physics. Cleveland, OH, CRC Press.

Lissant, K. J. (1983). Demulsification: Industrial Applications. New York, Marcel Dekker.

Myers, R. H. and D. C. Montgomery (1995). Response Surface Methodology: process and product optimization using designed experiments. New York, Wiley.

Otterstedt, J.-E. and D. A. Brandreth (1998). Small particles technology. New York, Plenum Press.

Qi, L., J. Ma, et al. (1998). "Micrometer-Sized Mesoporous Silica Spheres Grown under Static Conditions." Chemistry of Materials **10**: 1623-6.

Tanev, P. T. and T. J. Pinnavaia (1995). "A Neutral Templating Route to Mesoporous Molecular-Sieves." Science **267**(5199): 865-7.

Terry, T. L. (2001). Environmentally Benign Particle Synthesis by Electrdispersion Precipitation. Department of Chemical Engineering. College Park, University of Maryland**:** 84.

Tranter, R. L., Ed. (2000). Design and Analysis in Chemical Research. Sheffield Analytical Chemistry. Boca Raton, CRC Press.

Wedlock, D. J. (1994). Controlled Particle, Droplet, and Bubble Formation. Boston, Butterworth-Heinemann.